EXISTENCE OF A TRIPLE LAYERED SYSTEM OF "CA-GENERATORS" IN SWINE PURKINJE CELLS

REBECCA ELIZABETH DANIELS

Existence of a Triple Layered System of "Ca-Generators" in Swine Purkinje Cells

February 2013

Rebecca Elizabeth Daniels

A thesis submitted to the School of Graduate Studies in partial fulfillment of the requirements for the degree of Master of Science Division of Biomedical Sciences, Faculty of Medicine Memorial University of Newfoundland, St. John's, Newfoundland.

Abstract

Background: Spontaneous electrical signals from cardiac Purkinje fibers trigger life threatening arrhythmias. This abnormal signaling was associated with increased spontaneous intracellular Ca^{2+} activity following myocardial infarction. The present study aimed to understand the Ca^{2+} cycling within the endoplasmic reticulum (ER) in Purkinje cells (Pcells) in the large mammalian heart.

Methods: Immunofluorescence, electron microscopy, and fast confocal Ca^{2+} imaging were used with normal porcine Pcells, to examine the Ca^{2+} activity under various conditions including addition of specific agonist/antagonists of ER-Ca^{2+} channels.

Results: Spontaneous Ca^{2+} activity was different between 3 distinct subcellular regions: 1) the "Near SL" region was in close apposition with the sarcolemma (SL) and contained IP_3R_1; 2) the "SubSL" region, contained a thin layer of RyR_3, and 3) the core region contained RyR_2.

Conclusions: These results are consistent with the existence of 3 distinct layers of ER Ca^{2+}-generators in porcine Pcells, which highlights potential new mechanisms for Purkinje arrhythmogenicity.

Acknowledgements

I would like to express immense gratitude to my supervisor Dr. Bruno Stuyvers, for countless hours of instruction and support. This has been an arduous task, but you've been with me for every step of the way and I appreciate that more than I can articulate.

I would also like to thank the Faculty and Staff of the Division of BioMedical Sciences and the School of Graduate Studies at Memorial University. As well, I would like to thank the Canadian Institutes for Health Research (CIHR) for funding support.

Table of Contents

List of Figures

List of Tables

List of Abbreviations

2APB: 2-aminoethyl di-phenyl-borinate

ANEPPs: AminoNaphthylEthenylPyridinium; voltage sensitive sarcolemmal dye

AP: action potential

CICR: calcium-induced calcium-release

CVD: cardiovascular disease

DHPR: dihydropyridine receptor

DMSO: dimethyl sulfoxide

ECC: excitation contraction coupling

FWHM: full width half max

HEPES: (*4-(2-hydroxyethyl)-1-piperazineethanesulfonic acid*)

Ig: immunoglobulin

IP3/BM: rac-myo-inositol 1, 4, 5-triphosphate hexakis (acetoxymethyl) ester

IP_3R: inositol triphosphate receptor

MEM: modified eagles medium

MI: myocardial infarction

NCX: sodium/calcium exchanger

Pcell: Purkinje cell

PVT: polymorphic ventricular tachycardia

RyR: ryanodine receptor

SERCA: sarco-endoplasmic reticulum ATP-ase

SL: sarcolemma

SR: sarcoplasmic reticulum

TEM: transmission electron microscopy

T-Tubule: transverse tubule

RF: radiofrequency

Introduction

The Heart and Stroke Foundation of Canada reports that every seven minutes, someone in Canada dies from heart disease or stroke. Cardiovascular disease is the leading cause of death in Canada, and accounted for 29% of all deaths in 2004. Of these incidents, 23% were due to heart attacks (*Heart & Stroke Foundation, 2008*). 'Heart attack' is the common term for myocardial infarction (MI). MI occurs when a region of the heart does not receive adequate oxygen and becomes ischemic and dies. Survivors of MI are at an increased risk of sudden cardiac death, with the highest incidence in the first year after infarction. The major cause of these sudden deaths is occurrence of ventricular tachycardia (VT), a form of cardiac arrhythmia which frequently leads to lethal ventricular fibrillation (*Bigger et al., 1984*). VTs are believed to originate through triggered electrical activity and abnormal automaticity (*Arnar et al., 1997*). Abnormal electrical activity in cardiac Purkinje strands has been observed to occur before premature ventricular muscle activity during early ischemia, suggesting that spontaneous VTs have a Purkinje cell (Pcell) based origin (*Arnar et al., 1997*).

Haissaguerre and collaborators (2004) have reported that ablation of subendocardial Purkinje strands at the 'border zone' of an MI abolished the risk of resultant polymorphic ventricular tachycardia (PVT). This provided a clinical link between the Purkinje tissue overlying the infarcted region and the origin of PVTs (*Szumowski et al., 2004*). In a canine model of MI, Pcells survived the ischemic conditions, but had increased spontaneous intracellular Ca^{2+}-transients. These

spontaneous Ca^{2+}-transients occurred as large Cell Wide Ca^{2+} Waves (CWWs) which travelled from cell to cell in the Purkinje fibers. These Pcell aggregates exhibited a 70% increase in the incidence of CWWs after MI (*Boyden et al., 2003*).

Previous investigations of the relationship between spontaneous intracellular Ca^{2+}-variations and electrical activity of Pcells have found that: 1) the spatiotemporal aspects of excitation contraction-coupling (ECC) in Pcells differs greatly from those observed in the 'classical model' of ventricular myocytes *(Boyden et al., 2000)*; 2) Ca^{2+}-waves propagate through the Pcell aggregate via Ca^{2+}-Induced Ca^{2+}-Release (CICR); and 3) Large CWWs can elicit spontaneous, non-driven action potentials (AP) *(Boyden et al., 2000)*. From these findings, Boyden and colleagues hypothesized that spontaneous Ca^{2+}-waves are an arrhythmogenic mechanism in post-MI Purkinje tissue *(Boyden et al., 1989, 1994, 2000, 2003)*. In addition to the finding that the frequency of spontaneous Ca^{2+}-activity significantly increased in the post-MI canine model *(Boyden et al., 2003)*, these publications emphasized that very little was known about Ca^{2+} handling in Pcells from the normal heart.

In 2005, Stuyvers and collaborators proposed a structural and functional model of Ca^{2+}-activation in the normal Pcell (*Stuyvers et al., 2005*). The model was based on 3 layers of sarcoplasmic reticulum (SR) Ca^{2+} channels: 1) a layer composed of channels associated with type 1 inositol triphosphate (IP_3) receptors (IP_3R_1) directly under the sarcolemma, 2) a second layer of type 3 ryanodine receptors (RyR_3s), which extends about 6μm under the sarcolemma, while 3) the type 2 ryanodine receptor (RyR_2), the

unique form of SR Ca^{2+}-channels in myocytes, was present throughout the cell SR. Fluorescence Ca^{2+}-imaging revealed non-propagating Ca^{2+}-transients throughout the Pcell; these were termed 'sparks'. As well, this imaging showed propagating Ca^{2+}-events in the form of small Ca^{2+}-'wavelets' which were limited to a region ≈6μm depth under the sarcolemma; and large Ca^{2+} waves (*Cell Wide Waves; CWWs)* that travelled throughout the cell. The CWWs were believed to correspond to the arrhythmogenic activity observed in post-MI hearts. Immunofluorescence using specific antibodies showed that the highly organized distributions of RyR_2, RyR_3 and IP_3R_1 matched well the localization of Ca^{2+} sparks, wavelets and CWWs. Therefore, the researchers had demonstrated that CWWs could have resulted from the sequential activation of these SR Ca^{2+}-release channels.

Research Questions

A better understanding of the cellular origin of PVT could improve the control of arrhythmias and therefore improve the protection of patients undergoing severe MI. With this greater understanding, one could produce a reliable model of the cellular mechanism of activation in Pcells, which is critical in understanding and controlling PVT. Although the current version of the triple layered model of Ca^{2+}-activation improves our understanding of the cellular origin of PVTs, several assumptions in the model require experimental validation. The current study intends to address questions arising from the triple layered model of Ca^{2+}-activation (Stuyvers et al. 2005).

The triple layered system of Ca^{2+}-generators has been proposed to explain the (Centripetal) activation of canine Pcells; however, it is unclear as to whether the model can be applied to large mammalian species other than the dog, such as the pig. If so, this could have relevance for arrhythmias in the human heart since the human heart is anatomically very similar to that of the pig *(see Background Section 6 – The pig as a model for the human cardiovascular system).* Another question regarding the Centripetal Activation model relates to the potential expression of RyR_3 in Pcells in large mammalian hearts. RyR_3 were found predominantly in a peripheral subcellular region that specifically generated small waves (wavelets). This observation led to the proposal of an intermediate layer of RyR_3, called the SubSarcolemmal (SubSL) compartment. A distinct layer of SR Ca^{2+}-channels is an important determinant of the model because it would link membrane excitation to SR-Ca^{2+} release in the center of the cell. We attempted to determine whether experimental evidence supported the existence and function of such a RyR_3-based SubSL compartment in large mammalian Pcells.

Working Hypothesis

An intermediate layer of SR Ca^{2+}-channels exists in the porcine cardiac Purkinje fiber linking excitation of the sarcolemma with SR Ca^{2+}-release in the core. Excitation of the sarcolemma initially causes peripheral SR Ca^{2+}-release, which is linked through an intermediary layer of RyR_3 to a large release of SR Ca^{2+} in the cell centre and the formation of large Ca^{2+}-transients, such as CWWs.

Experimental Approach

Prior to addressing the above hypothesis, we needed to confirm that porcine Pcells have similar characteristics to those previously reported for canine Pcells. In particular, it was necessary to determine if porcine Pcells were anatomically distinct from porcine ventricular myocytes and therefore, like canine Pcells, could not be studied based on the well-known myocyte model (*via excitation contraction-coupling. See Background section 3, page 9 for more information*).

Aim1: It was crucial to determine if, like canine Pcells, porcine Pcells lack transverse tubules (T-tubules). T-tubules consist of inward projections of the cell membrane. T-tubules contain abundant dihydropyridine receptors (DHPR). The T-tubules couple Ca^{2+}-entry through the DHPRs with Ca^{2+} release from RyRs in the SR membrane, thereby producing a uniform intracellular Ca^{2+} increase upon membrane depolarization. It is possible that the absence of T-tubules in porcine Pcells may be compensated in the cell activation process by the Centripetal Ca^{2+}-Activation as proposed previously in the canine Pcells *(Stuyvers et al., 2005).*

Aim 2: In the canine model, RyR_2 and IP_3R_1 were found in specific regions of the Pcell: the core and peripheral regions, respectively *(Stuyvers et al., 2005).* Aim 2 examined the regional specificity of SR-Ca^{2+} channels in porcine Pcells.

Aim 3: In the canine model, Stuyvers et al. (*2005*) described small propagating Ca^{2+}-transients (wavelets), occurring in the SubSL SR-region expressing RyR_3. The first part

of Aim 3 determined if the same intermediate layer of RyR_3 was present in porcine Pcells.

Also, it has been reported that canine *(Boyden et al.,2000)* and rabbit (*Cordiero et al., 2001; Spitzer et al., 1997*) Pcells loaded with a fluorescent Ca^{2+}-indicator respond to electrical excitation with an initial increase in fluorescence at the periphery, followed by an increase in the core. In contrast, ventricular myocytes under the same conditions displayed a uniform Ca^{2+}-increase. To verify that porcine Pcells had the same feature, Pcells were field stimulated and the "Ca^{2+}-response" was compared with that of ventricular myocytes in the same conditions.

Intracellular Ca^{2+}-activity was assessed at different extracellular Ca^{2+}-concentrations (Ca_o) in the second portion of Aim 3. Murayama et al. reported that the threshold of activation for RyR_3 is 0.1-1μM cytosolic Ca^{2+}(1999), which is much lower than that of RyR_2, which is 3mM cytosolic Ca^{2+} *(Kong et al. 2008).* Therefore, for the final part of Aim 3 in our study we examined the location of Ca^{2+}-transients at 4 different Ca^{2+}-concentrations (1, 2, 4, and 8mM) and attempted to identify specific regions of Ca^{2+}-activity which would correlate with RyR_2- and RyR_3-Ca^{2+}-thresholds respectively.

Aim 4: To test further the existence of specific regions of SR Ca^{2+}-channels in Pcells we used selective pharmacological agonists/antagonists. Dantrolene, which specifically inhibits RyR_3, was used to localize any changes in Ca^{2+}-cycling that might occur. Changes in Ca^{2+}-dynamics within cells exposed to this drug indicated the existence and location of RyR_3 in these cells. 2APB and Xestospongin-C, which are specific inhibitors

of IP_3R, were used to localize these receptors. IP_3/BM which activates IP_3R_1 was used to further clarify the location and function of the IP_3Rs.

Background

1-Post-MI Arrhythmias can originate in cardiac Purkinje fibers

Sudden cardiac death is a lethal consequence of coronary artery disease and accounts for about 50% of mortalities from cardiovascular disease (CVD) in developed countries (*Reddy and Yusuf, 1998*). Approximately 80% of deaths related to CVD occur in the first 6-18 months after an MI in a predictable sequence of events. Initially, there is VT which, when left untreated, degenerates to ventricular fibrillation (VF) and then leads to the terminal step: sudden cardiac death, which is complete asystole (*Zipes et al. 1998; Huiikuri et al., 2001*).

Clinical studies frequently associate PVT with the area of infarcted tissue that is damaged (*Bode et al. 2008; Szumowski et al., 2004*). A particular method of treatment in patients with persistent abnormal cardiac rhythm involves surgically administering a radiofrequency (RF) catheter to ablate this area of infarcted tissue. RF catheter ablation therapy is reported to have been successful in patients with persistent electrocardial abnormalities such as triggered monomorphic ventricular premature beats, which often precede PVT, and frequent episodes of VF. In patients with coronary artery disease (CAD), the most successful ablation site was located at the Pcell network near the edge of the MI scar. Following ablation at this site, there was no recurrence of VT or VF (*Bode et*

al. 2008; Szumowski et al., 2004). These clinical studies provide support for the hypothesis that the Purkinje network is fundamental in the initiation of arrhythmogenesis.

2- The Purkinje fibers can generate Spontaneous Electrical Activity in the heart

The study of arrhythmogenesis in animal models has confirmed that Pcells exhibit spontaneous action potentials (AP). These APs perturb normal cardiac rhythm and contribute to the abnormal cardiac mechanisms involved in arrhythmias. Large spontaneous Ca^{2+}-transients can occur without any external stimulation. These are electrogenic currents, consisting of intracellular elevations of Ca^{2+} which activate the depolarizing current I_{ti}. This depolarizes the membrane potential and creates a spontaneous AP (*Boyden et al. 2000*). As mentioned above, in post-MI conditions there is a 70% increase in the frequency of these spontaneous CWWs (*Boyden et al. 2003*). When the normal Ca^{2+}-cycling in Pcells becomes disordered and these APs are created out of sync with the normal heart rhythm, the necessary signal propagation between cells is compromised, potentially beginning the arrhythmogenic cascade to PVT and death. As described above, RF catheter ablation studies have shown that physical ablation of these post-ischemic Pcells dramatically reduces the likelihood of future PVTs (*Bode et al., 2008; Szumowski et al., 2004*).

Linking these clinical findings with those of biomedical research *(Boyden et al. 2000, 2003*), it becomes apparent that the problem of lethal arrhythmogenesis following MI begins with dysfunction within the cardiac Purkinje network. However this network,

under normal healthy conditions, has not yet been described. In order to understand the origin of these arrhythmogenic Ca^{2+}-waves and the mechanism through which they increase in the post-MI heart, it is essential to understand the physiology and mechanism of activation in normal Pcells.

3- Classical Model of Cardiac Excitation-Contraction Coupling (ECC) in Ventricular Myocytes

Ventricular myocyte contraction begins with the depolarization phase of the AP. This depolarization of the sarcolemma causes a conformational change in the voltage sensitive DHPRs and allows for an influx of Ca^{2+}. This influx activates the RyR, which are Ca^{2+}-release channels on the SR, evoking a large release of Ca^{2+} into the cytosol, causing a conformational change in the troponin-tropomyosin complex of the sarcomere and an active generation of force. This force is observed as the contraction of the myocyte and is reversed when the Ca^{2+} is pumped back into the SR by the Sarco/Endoplasmic Reticulum ATPase (SERCA) isoform 2a and out of the cell through the Sodium/Calcium exchanger (NCX) (*Katz, 1992*).

During the depolarization phase, opening of the DHPRs allows the Ca^{2+} to enter the cell through the T-tubules (Fig. 1). This is important because T-tubules allow the uniform intracellular distribution of Ca^{2+} ionic currents, allowing for uniform activation of RyR within SR of these myocytes (*Katz, 1992*).

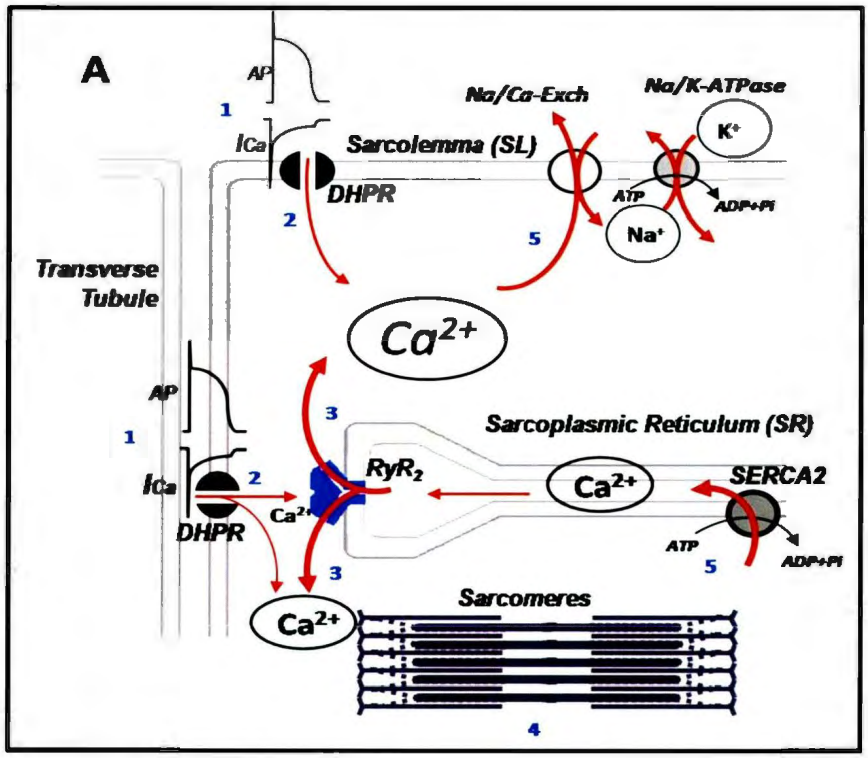

Figure 1: Schematic diagram of the Classical model of Calcium Induced Calcium Release (CICR) in Ventricular Myocytes. Na/K-ATPase=membrane bound Na^+-K^+ exchange pump; Na/Ca-Exch=membrane bound Na^+-Ca^{2+} exchange pump; SERCA2=Sarco/Endoplasmic Reticulum Ca^{2+}-ATPase; DHPR=Dihydropyridine Receptor; I_{ca}=inward flow of Ca^{2+} *(Image Source: Stuyvers BD, 2009)*

4- Excitation-Activation Coupling in Cardiac Purkinje Cells: How this happens without T-Tubules

Cardiac Pcells from 'larger' mammals such as rabbits (*Cordiero et al., 2001*) and canines (*Stuyvers et al. 2005*) have been reported to lack T-tubules.

The T-tubule may increase the cells total capacitance, thereby delaying the speed of sarcolemmal depolarization and reducing the conduction velocity of AP transmission. This would hinder the rapid conduction of electric signal between cells. The absence of T-tubules in Pcells could facilitate faster AP conduction (*Di Maio et al., 2007*). In myocytes, the T-tubular system permits the rapid spread of Ca^{2+}-trigger signal through the interior of the cell. Therefore, the Pcell must have a fundamentally different

mechanism linking activation of intracellular Ca^{2+}-proteins with plasma membrane excitation *(Coridero et al., 2001)*.

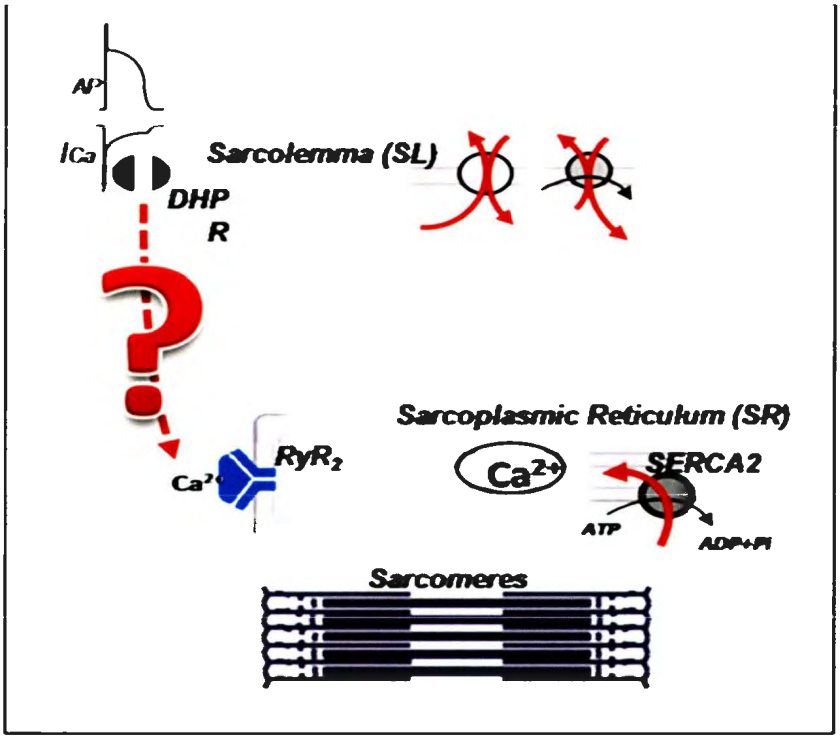

Figure 2: Schematic diagram of ECC in Pcells of a large mammalian heart. Question mark refers to the unknown mechanism through which these cells link excitation of the membrane with activation of internal proteins. RyR=Ryanodine Receptor; DHPR=Dihydropyridine Receptor *(Image Source: Stuyvers BD, 2009).*

5-Proposed Mechanism Linking Plasma Membrane Excitation with Pcell SR Activation in Large Mammalian Hearts

Stuyvers and collaborators *(2005)* have proposed a structural and functional model of cellular activation to explain the unique method of ECC in Pcells from large mammalian hearts. The model is based on 3 layers of SR Ca^{2+} channels: 1) type 1 IP_3 receptors (IP_3R_1) directly under the sarcolemma (SL), 2) type 3 ryanodine receptors (RyR_3), which extend about 6µm under the sarcolemma, while 3) type 2 ryanodine receptors (RyR_2), classical SR Ca^{2+}-channel in myocytes, are present throughout the cell with the exception of a SubSL void region, 2µm wide (Fig 3).

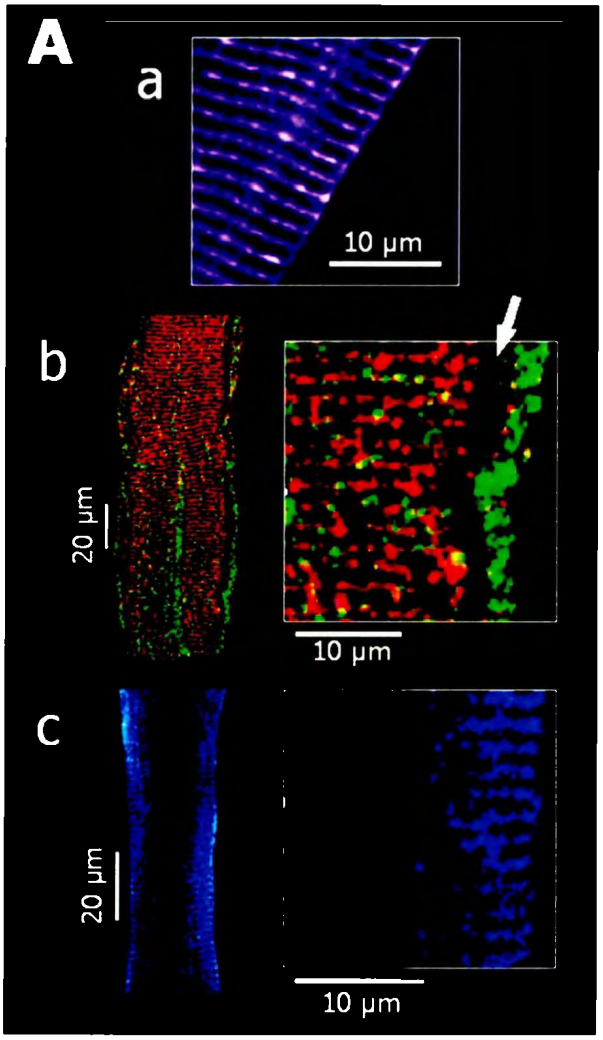

Figure 3: Results from the localization of SR Ca^{2+} channels in canine Pcells. Pcells are labeled for: a) all isoforms of RyR b) IP_3R_1 (green) and RyR_2 (red); and c) RyR_3. The RyR antibody stained uniformly throughout the cell, exhibiting transverse striations of approximately 2-µm, IP_3R_1 formed a thin layer 1.91 ± 0.49-µm located directly under the sarcolemma. RyR_2 is distributed throughout the cell in transverse striations with a periodicity of 1.9 ± 0.2-µm with the exception of an apparent void region, 2-µm in width (1.9±0.2-µm) between the sarcolemma and the cell centre (see white arrow (b)). Neither IP_3R_1 nor RyR_2 were found in this region. The RyR_3(blue) antibody also exhibited the same 1.9 ± 2-µm transverse striations and was found only at the periphery of the cell, extending approximately 6 to 7-µm from the sarcolemma, over the apparent void region. ***(Reproduced with permission by Stuyvers et al., Circulation Research 2005; Fig. 5, modified)***

Fluorescence Ca^{2+}-imaging revealed the existence of three distinct types of Ca^{2+} waves, which matched well the highly organized distribution of SR Ca^{2+}-release channels. The first type, which occurs directly below the sarcolemma, is a small, non-propagating Ca^{2+}-transient. When several of these occur at the same time, they contribute

to small Ca^{2+}-waves (termed 'wavelets') in the SubSL region, which are limited to approximately 6μm depth under the plasma membrane. This region is populated with IP_3R_1 and RyR_3 (Fig. 3). RyR_3 have shown to generate Ca^{2+}-sparks, even in an unstimulated cell and because of their low threshold of activation, RyR_3 will readily respond to Ca^{2+} release by generating wavelets in the SubSL region. As mentioned above, Murayama and collaborators report that the threshold of activation for the RyR_3 is between 0.1and 1μM luminal Ca^{2+} *(1999)*. These small Ca^{2+} wavelets accumulate and trigger large CWWs, which propagate through the cell from end-to-end. CWWs are proposed to be the result of many RyR_2 Ca^{2+}-release channels *(Stuyvers et al., 2005)*, which have a significantly higher threshold of activation at approximately 3mM luminal Ca^{2+} *(Kong et al., 2008)*.

From these observations, investigators proposed a model of Centripetal Activation in Pcells from large mammalian hearts (Fig. 4). Here, large sparks in the SubSL region activate RyR_3-proteins which create small Ca^{2+}-wavelets. If conditions are different from normal, such as during stimulation or following an MI, wavelets can activate central RyR_2s leading to large, electrogenic CWWs. This electrogenic activity perpetuates from cell to cell within an aggregate *(Stuyvers et al., 2005)*.

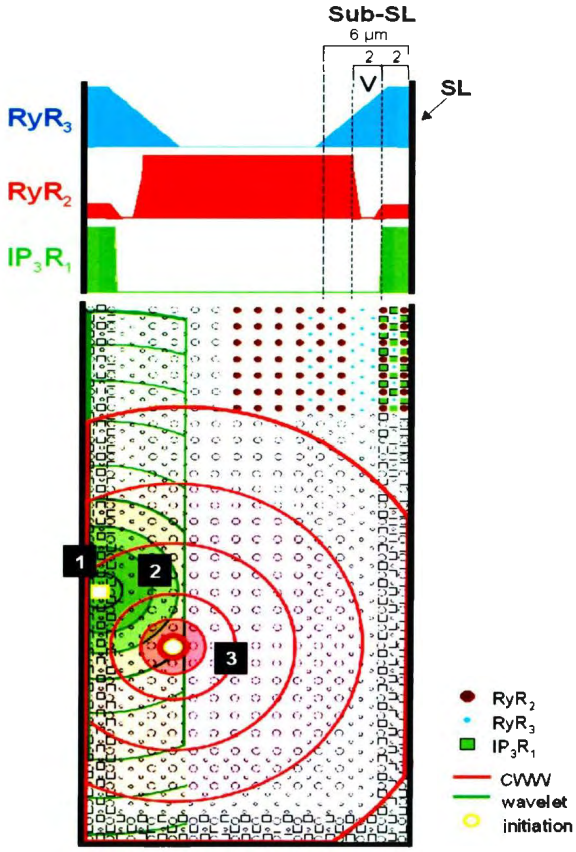

Figure 4: Model of Centripetal Activation of Pcells in large mammalian hearts. This model is based on the triple layered system of SR Ca^{2+}-channels. On the panel at the top of the figure; at the periphery of the SR, the first layer consists of IP_3R_1 (green squares) directly under the cell membrane which overlaps with the outer edge of the second layer, the RyR_3 (blue circles). The cell centre contains very few IP_3R_1 and virtually no RyR_3, but is filled with RyR_2 (dark red circles). These form the third layer, at the core of the Pcell. There are some RyR_2 contained in the first, 'SubSL' layer along with the IP_3R_1. RyR_2 is absent in a SubSL void (V) section between the first and third layers. Below the void, RyR_2 and RyR_3 overlap. *(Reproduced with permission by Stuyvers et al. Circulation Research 2005)*

Although the current model of the Centripetal Activation contributes to further understanding of the cellular origin of PVTs, several assumptions in the model still require an experimental validation.

Assumption 1: The canine model can be applied to other large mammalian species.

Assumption 2: Canine Pcells differ morphologically from ventricular myocytes, so the same must be true of other large mammalian species.

The next sections relate to what is known and what is left unanswered regarding these questions.

6-The Pig Heart as a Model for the Human Cardiovascular System

The Yucatan mini pig was used to test if the model of Centripetal Activation applies to large mammals other than the dog. Pigs are considered to be a valuable model for human cardiovascular research because physiologically and anatomically they are very similar to humans. This is applicable to cardiovascular function, digestion, and they can have a comparable body mass. With regard to cardiovascular function, pigs have similar heart-to-body ratios as humans; they also have similarly sized coronary arteries and a comparable collateral circulation (*Carey GB., 1997*). Given these anatomical similarities, porcine cardiac valves are used to surgically replace malfunctioning valves in humans. Additionally, the porcine cardiac conduction system is made up of a dense network of Purkinje fibers. It is considered to be well developed and representative of the human system (*Crick SJ et al., 1999*).

7- The cardiac Purkinje cell, what is known?

Pcells are specialized, rapidly conducting extra-nodal cells of the heart which exist in discrete bands in the ventricular chambers and in the atria. In humans, Pcells are 70-80μm in diameter and are the broadest cells in the heart. Pcells have an abundance of linearly arranged sarcomeres, in a homogenous pattern similar to that of the ventricular myocytes (*Legato, 1973*). Actin filaments and myosin proteins comprise sarcomeres, the contractile unit of the cell. Sarcomeres are arranged in long filaments, termed myofibrils

(*Katz. 1992*). Under electron microscopy, Pcell myofibrils may be interrupted by large, seemingly clear pools of sarcoplasm filled with glycogen particles, mitochondria, and SR tubules (*Legato. 1973*). The finding that Pcells have well ordered sarcomeres is puzzling because their principal function is not contraction, but rather the intercellular propagation of the AP. One possible explanation is that these sarcomeres are remnants of the differentiation program that Pcells share with myocytes, during development of the organism (*Di Maio et al. 2007).*

Pcells from cats, rabbits, guinea pigs, goats and sheep all exist in aggregates that are more tightly packed in the larger animals (*Sommer and Johnson, 1968*). They show a large variation in diameter between species, which may be partially due to the junctional complexes through which they fuse together (*Sommer and Johnson, 1968*). Pcell intercalated discs have a typical structure of long finger-like projections, obliquely running membranes, and numerous desmosomes associated with intermediate filaments. This is in contrast to the step-wise disposition and transversely oriented adhering junctions present in ventricular myocytes (*Di Maio et al., 2007*).

The SR of Pcells is similar to that of ventricular myocytes, which is composed of two domains. The Ca^{2+}- pumping SR forms a loose network around the myofibrils. The junctional SR (jSR) has two configurations: flat cisternae associated with the sarcolemma, and the spherical corbular SR, with no sarcolemmal attachments (*Di Maio et al., 2007*). In Pcells, the SR Ca^{2+}-release channels in the SubSL cisternae control the electrical Ca^{2+} influx which initiates systole, causing contraction of the heart, while the

extensive sarcotubular network contains a densely packed system of SERCA-2a that function in diastole, facilitating relaxation of the heart *(Katz, 1992)*.

8- Molecular components of the SR-Ca^{2+} release in Pcells

Ryanodine Receptors

The principal SR Ca^{2+}-release channel is the RyR. These are large, tetrameric proteins. Each of their four subunits contains a cytoplasmic domain (the "foot") and at least four α-helical membrane spanning segments. When the RyR is open, there is a central pore in the transmembrane region that is connected to the 4 subunits. When the channel is closed, the central pore and the subunits are no longer connected *(Katz, 1992)*.

Pcells from large mammalian hearts contain RyRs as components of the jSR at peripheral couplings or the corbular SR (*Di Maio et al., 2007, Cordiero et al., 2001*). Immunofluorescence specific for RyR_2 in rabbit ventricular myocytes exhibits striations, corresponding to the location of the T-tubule region. Surprisingly, Pcells also exhibit striations of RyR_2 in this region, similar to those in ventricular myocytes *(Coridero et al., 2001)*.

RyR Isoforms

There are three main isoforms of RyR: RyR_1 which is found predominantly in skeletal muscle, RyR_2 which is often referred to as the 'cardiac isoform' and RyR_3, which has wide distribution throughout the tissues of the body. RyR_3 was originally described in the brain, and therefore is sometimes referred to as the 'neural isoform' *(Zucchi and Ronca-Testoni, 1997)*.

The Inositol Triphosphate Receptor (IP_3R)

IP_3Rs are much smaller than RyRs. They open and close much more slowly, and are found primarily in smooth muscle. The function of these channels in the heart is not well defined, but it is hypothesized that they may help to regulate resting tension or cellular processes such as protein synthesis, cell cycling, or apoptosis *(Katz, 1992)*. IP_3Rs in cardiac Pcells are associated with large, local Ca^{2+}-elevations and are densely concentrated under the SL and perinuclear regions (*Hirose et al., 2008*). It has been proposed that IP_3Rs have a role in gene transcription and other cellular processes in Pcells, and that they can mobilize large stores of Ca^{2+} under neurohormonal stimuli *(Hirose et al., 2008)*.

9- Cardiac Cellular Response to Electrical Stimulation: Pcells versus Ventricular Myocytes

When rabbit ventricular myocytes are electrically stimulated, the resulting Ca^{2+}-release is observed synchronously across the cell. In rabbit Pcells, electrical stimulation causes a Ca^{2+}-release at the cell edge preceding that in the centre (*Cordiero et al., 2001*). This is reflective of what is seen in the canine Pcell model: upon electrical stimulation, Ca^{2+}-transients occur along the periphery, as well. In rabbit and canine Pcells, the initial peripheral Ca^{2+}-transient induces another transient, which propagates uniformly toward the core of the aggregate. Spontaneous Ca^{2+}-transients begin at one end of the aggregate during the evoked AP, and travel along the length of the aggregate *(Boyden et al., 2003)*.

Only cells which lack T-tubules, such as Pcells respond to electrical stimulation by an initial Ca^{2+}-release at the periphery. In these cells, Ca^{2+} is released just below the

surface of the cell membrane, which can then move into the interior by diffusion and CICR (*Stuyvers et al., 2005*). By contrast, in ventricular myocytes, the T-tubules provide physical contact between the opening of the DHPR upon membrane depolarization and the activation of SR Ca^{2+}-channels deep inside the cell. This allows for a synchronous, uniform Ca^{2+}-release (*Brette et al. 2006*).

10- Hypothesis to Explain the Differences Observed in the Activations of Pcells and Myocytes: A Cellular Defense Mechanism?

Potential explanations for the peripheral SR Ca^{2+} release following electrical stimulation in rabbit Pcells were proposed by Cordiero and collaborators (*2001*). They hypothesized that the RyRs in the cell centre were silent and therefore did not contribute to the electrically evoked Ca^{2+}-transient. The junctional RyRs at the periphery were exposed to higher resting Ca^{2+}-concentrations and therefore reacted more readily to the electrical stimulus. As a result, Ca^{2+}-sparks arose from clusters of RyRs which are only present at junctions between the surface membrane and the SR. From these potential explanations, researchers conjectured that the clusters of RyRs in close apposition with the sarcolemma provide stable spatial separation of the excitation at the level of the sarcolemma, and activation of the core RyRs (*Cordiero et al., 2001*). Cordiero and collaborators theorize that the lack of T-tubules may be a physiological defense mechanism in the Pcell: uncoupling the central RyRs from the influx of Ca^{2+} after excitation of the membrane would prevent uncontrolled release and the resulting electrical disturbances. Because the Purkinje system is essential in proper cardiac

conduction, this uncoupling may be an important modification to reduce the likelihood of abnormal electrical activity *(Cordiero et al., 2001)*.

11- Pharmacological Approach to the SR-Ca^{2+} channels

Does the usage of pharmacological agents which specifically inhibit or activate RyR_3 support the existence of the SubSL region? Does the usage of pharmacological agents specific for IP_3R_1 or RyR_2 support the existence of a triple layered system of Ca^{2+}-activation in porcine Pcells, as described in canine Pcells?

In cardiac Pcells and ventricular myocytes, spontaneous Ca^{2+}-sparks may be completely inhibited by the SERCA inhibitor thapsigargin. Exposure to the DHPR blocker nifedipine did not decrease the number of Ca^{2+}-sparks. Together, these results indicate that the spontaneous Ca^{2+} sparks are not initiated by a Ca^{2+}-influx via DHPRs; rather, this is non-driven Ca^{2+} release from the SR (*Cordiero et al., 2001*).

RyR_3 Inhibition

Dantrolene is a commonly used muscle relaxant that affects cardiac ECC (*Salata and Jalife, 1982*), but its mechanism of action is unclear. Dantrolene has been applied to canine P-fibers to change the properties of the AP, and may be administered to patients experiencing ventricular arrhythmias during anesthetic-induced Malignant Hyperthermia (*Salata and Jalife, 1983*). An association has been drawn between the effects of dantrolene and the RyR. Dantrolene is typically administered to calm chronic skeletal muscle spasticity. Skeletal muscle has a high density of RyR_1 (*Kraus et al., 2004*). As

well, dantrolene significantly inhibits RyR_3 while having no effect on RyR_2 (*Zhou et al., 2001*).

Stuyvers and collaborators were able to inhibit Ca^{2+} activity in canine Pcells, which were found to lack RyR_1 but contained RyR_2 and RyR_3 (*Stuyvers et al., 2005*). An inhibition of Ca^{2+}-activity in porcine Pcells, in the presence of dantrolene could be a validation of the presence of RyR_3 in these cells.

IP_3R_1 Inhibition

The effects of pharmacological agents specific for IP_3R in canine Pcells have been examined. 2APB, a modulator of IP_3-sensitive Ca^{2+} release channels caused a significant reduction in the quantity of Ca^{2+} wavelets and SubSL sparks (*Stuyvers et al., 2005; Hirose et al., 2008*). This provided support for the hypothesis that IP_3Rs are located in the region just inside of the sarcolemma of the Pcell (*Stuyvers et al. 2005; Hirose et al. 2008*). Phenylephrine, an α-adrenergic agonist, has been shown to increase the production of IP_3. Application of this compound resulted in an increase in the rate of large Ca^{2+}-sparks by 97% in the SubSL; while it had no effect on transient Ca^{2+}-events (TE), which are thought to be the result of RyR_2 Ca^{2+}-release (*Hirose et al. 2008*). U-73122, an inhibitor of phospholipase C (PLC) which is involved in the production of IP_3, abolished large SubSL Ca^{2+}sparks. When 2APB was used in conjunction with phenylephrine, no significant effect was observed on the spark frequency, indicating that 2APB blocks the effect of the phenylephrine. From these results, the authors suggested that large, SubSL spark production was sensitive to IP_3R blocking agents, providing support for the theory that IP_3Rs are the cause of these large Ca^{2+}-sparks (*Hirose et al., 2008*).

12- Background of Methods of Assessment of the Excitation-Activation Coupling

2D Confocal Microscopy

Scanning laser confocal microscopy enables cellular physiologists to view a cell or tissue in entirety, without directly affecting its shape or function. This is particularly useful for examination of live cell cultures, maintaining the integrity of the plasma membrane and allowing for visualization of the normal proteins and ongoing cellular mechanisms (*Guthoff et al., 2009*). Confocal microscopy differs from traditional light microscopy in several ways. Light microscopy homogenously illuminates and then magnifies the image, which is then projected onto a detector, such as a camera or the eyepiece of the examiner. Light microscopy is not useful for optical sectioning because all structures, even those outside of the focal plane, will affect the intensity of the signal. This will reduce the contrast in the image and therefore, decrease the quality of the image (*Saggau, 2006*).

Confocal microscopy uses point detection by spatial filtering with a small aperture, called a "pinhole." This pinhole is 'confocally' aligned with light coming from the focal point of the desired region of sample, excluding other points of illumination. This method allows for optical sectioning of the sample, by blocking emission light which does not come from the specific illumination point being examined, via the pinhole. Therefore, examiners can visualize a very specific section of the 3D sample, without interference from neighboring structures (*Saggau, 2006*).

When this technique is used on larger tissue sample, which would scatter the light, a pinhole of small size in the emission pathway can significantly improve the spatial resolution by restricting the amount of light that the detector receives and thereby creating a clearer image (*Saggau, 2006*). However, because a portion of light is discarded as it passes through the beam splitter, increased illumination strength is required initially. Unfortunately, this causes photodamage in living tissue and cells (*Saggau, 2006*).

The Nipkow Spinning Disk

The Nipkow spinning disk allows for scanning with approximately 1000 laser beams and therefore, much faster than other forms of scanning laser confocal microscopy (*Advanced Imaging Concepts, 2010*). While it typically takes about one second to produce an image on a traditional confocal microscope, the Yokogawa CSU has a scanning speed of up to 360 frames/second(Yokogawa Electric Corporation, 1994-2012). With the appropriate video cameras and fast computer systems, this speed allows for imaging of live cell dynamics and protein interactions (Grant et al., 2007). With the Nipkow spinning disc, the laser beams pass through serial pinholes and the beam fills the aperture of the objective lens before being focused onto the focal plane. Fluorescence emitted from the specimen is captured by the objective lens and focused back onto the disc containing the pinholes. This fluorescence may then be transmitted through the same hole to eliminate any out of focus signals, deflected by a dichroic mirror (*Advanced Imaging Concepts, 2010*).

The Nipkow disc may be used to split the fluorescence signal from the reflected laser so that the beam will be passed through the emission filter and then be focused into the image plane, in the eyepiece or camera. This microlens array disc is connected to the Nipkow disc, so as they rotate, they scan the entire field of view at very high speeds. This enables users to record confocal fluorescent images in real time through the eyepieces of the CSU head. As well, because scanning by the CSU with multiple beams requires a significantly lower level of light intensity per unit area, photo bleaching and photo toxicity in live cells is significantly reduced (*Advanced Imaging Concepts, 2010*).

13- Immunofluorescence

Immunofluorescence has been used in the current study to characterize the nature and the distribution of the SR-Ca^{2+} channels in Porcine Pcells. Immunofluorescence techniques have a wide number of uses including the determination of cell types and the expression of pathological changes in tissues and cells.

The technique uses the specific interaction between the antibody and its antigen, coupled with methods of fluorescence imaging. Specific primary antibodies are used to recognize cellular antigens. Following their incubation period, secondary antibodies which contain a fluorescent fluorochrome are added. These secondary antibodies react with the primary antibody, and allow for its visualization using fluorescence confocal microscopy (*Wilkens A 2005*).

Materials & Methods

1- Heart Extraction

Yucatan miniature pigs were bred and raised on site at the Vivarium Pig Breeding Station of Memorial University. A total of 97 pigs were sacrificed: 26 females and 67 males; which ranged in size from 23 to 58 kg. On the day of experiments, the pigs received an intramuscular injection of ketamine (Ketalean®, 100mg/mL) at a dose of 22 mg/kg. Then they were intubated and anaesthetized with a combination of 10% isofluorane gas and oxygen. Intravenous heparin was given to reduce the likelihood of blood clots in the heart after excision. The chest cavity was opened, and the vessels surrounding the heart were clamped. The heart was extracted and immediately placed in Tyrode (pH 7.4, on ice) solution containing heparin. This Tyrode solution was oxygenated, and contained (in mM): NaCl 145, KCl 4, $MgCl_2$ 1, NaH_2PO_4 0.33, HEPES 5, Glucose 10, $CaCl_2$ 2.

All animal protocols were approved by the Institutional Animal Care Committee at Memorial University, in accordance with the guidelines of the Canadian Council on Animal Care.

2- Live PCell Isolation

Free running P-strands were dissected from the ventricular walls and placed in Kreb's Henseleit (K-H) solution with a pH=6.7 at 25°C, bubbled with 5% CO_2/95% O_2. Kreb's solution was brought to the pH of 6.7 with the addition of HCl. Strands were washed in fresh K-H, followed by MEM at 37°C. K-H solution contained (in mM): NaCl 118, KCl 4.7, KH_2PO_4 1.2, $MgSO_4$ 1.2, Na_2HPO_4 0.3, $NaHCO_3$ 24, Glucose 11.1. Modified

Eagle's Medium (MEM) solution contained (in mM): NaCl 137, KCl 4, KH_2PO_4 0.44, $MgSO_4$ 16, $NaHCO_3$ 4, Na_2HPO_4 0.3, Glucose 5.5, $MgCl_2 \cdot 6H_2O$ 5.5, HEPES 0.5, as well as MEM Amino Acid Solution (GIBCO 11130-051) and MEM Vitamin Solution (GIBCO 11120-052). Strands were incubated in MEM for 20 minutes, while oscillating at approximately 40 RPM, and bubbling with 5% CO_2/95% O_2. They were transferred into a collagenase solution: 25 mg Worthington Type 2 collagenase (294u/mg, cat#4177 lot#47A9338) in 6mL MEM, incubated at 37°C for 1 hour at an oscillation of 40 revolutions per minute (RPM). Following this incubation, supernatant was removed and replaced with MEM at 37°C. Isolated cells and aggregates were viewed under the light microscope to assess viability and quantity.

3- Sarcolemma Staining

Live Pcells were used immediately after isolation. They were stained with lipophilic, voltage sensitive, membrane specific Di-8-ANEPPS (Invitrogen D-3167). Here, a 2mM stock solution was prepared with di-methyl sulfoxide (DMSO, Sigma D8418) and stored at 4 °C, protected from light. Pcells were stained using a solution of 500 µL Ca^{2+} -free Tyrode, 2 µL Pluronic® F-127 Solution (Invitrogen P300MP) and 2 µL stock Di-8-ANEPPs solution, mixed with 500 µL of cell suspension in Ca^{2+} free Tyrode. Cells were incubated in this dye solution for at least 5 minutes before slides were made on site. Cells were then observed using a Laser scanning confocal microscope (Olympus FV300). When bound to the phospholipid bilayer membrane, Di-8-ANEPPs had an absorption (Excitation) spectrum of 360-475 nm wavelength, while it has a fluorescence Emission of 500-750 nm wavelength. Therefore, following washout of dye, cells were excited at 488

nm and the emitted signal was recorded at 520 nm. Note that Excitation and Emission wavelengths matched those of Ca^{2+} dye Fluo4 (see above) and therefore, both staining experiments could be carried out simultaneously.

4- Electron Microscopy

Purkinje strands were stretched and pinned into paraffin wax, immediately following isolation. Strands were stretched to remove slack so that sarcomeres were set at their resting length (no load). Immediately following this, Pstrands were fixed in Karnovsky fixative. The fibers were then transferred to 1 M sodium cacodylate buffer. The tissue was then dehydrated and infiltrated using the following method, with the entire process taking place on a rotator: The tissue was placed in 1% osmium tetroxide, 1M Na Cacodylate Buffer, then dehydrated by being placed sequentially in: 70% ethanol, 95% ethanol, absolute ethanol, and absolute acetone. Subsequently, the tissue was infiltrated using 50:50 acetone and resin, and TAAB 812 Resin. The fibers were then embedded in BEEM capsules and polymerized overnight at 80°C. Blocks were trimmed and then 0.5 µm sections were cut using a diamond knife on a Reichert Ultracut S microtome. Sections were mounted on glass slides, dried in a hot place, and subsequently heat fixed and stained with 1% Toluidine blue in 1% boric acid. Thin sections of 90 nm were cut using the Reichert Ultracut S and a diamond knife. Sections were mounted on 300 mesh copper grids, which were then air dried for 30 min. Following this, they were stained with 3% uranyl acetate in 30% ethanol for 5 min, followed by 1% lead citrate stain for 5 min. The grids were rinsed with distilled water and air dried and then examined in a JOEL 1200 EX Transmission Electron Microscope. Images were recorded on Kodak electron

microscope film, developed, then scanned as digital images using an EPSON perfection V750Pro scanner and saved as JPEGs.

5- Immunofluorescence

Pcells were washed with phosphate buffered saline (PBS, GIBCO 10010-23) at 25 °C immediately after being isolated. Pcells were then fixed in a 2% formaldehyde solution (Aldrich 533998) for 15-35 minutes. After this, Pcells were washed with PBS and permeabilized in a 0.30% triton X-100 (Sigma Aldrich T9284) solution containing 1% bovine serum albumin (Sigma A2153), at 25 °C for 35 minutes. Pcells were then washed with PBS and covered in image enhancer solution (Invitrogen Image-iT®FX signal enhancer I36933) for 1 hour at 25 °C. This solution was used to block nonspecific fluorescence. Pcells were then washed with PBS and incubated with the primary antibody overnight at 4 °C, protected from the light.

On the next day, the cells were washed with PBS and then the secondary antibody was added, in a 1:200 dilution. This solution was then allowed to incubate at 4 °C, protected from the light for 2-6 hours, depending on the manufacturer's instructions. Following this cells were washed with PBS and then mixed with antifadent mounting medium (Citifluor 17972-100) before slides were made and examined using the Olympus FV300 scanning laser confocal microscope.

Primary Antibodies used: RyR (non-isoform specific, Affinity BioReagents Monoclonal Mouse/IgG1 Anti-RyR, dilution 1:100); RyR_2 (Affinity BioReagents Monoclonal Mouse/IgG1 Anti-RyR_2, clone 34C, 1:100; Abcam Polyclonal Rabbit Anti-RyR_2, dilution 1:1000); RyR_3 (Millipore Polyclonal Rabbit Anti-RyR_3, dilution 1:100;

IP_3R_1(EMDBiosciences/Calbiochem Mouse/IgG_{2b} Anti-IP_3R, clone IP_3R_1, dilution 1:100; Affinity BioReagents Rabbit Polyclonal Anti-IP_3R_1 (PA1-901), dilution 1:200); and for preliminary studies: α-Actinin (Affinity BioReagents Monoclonal Mouse/IgG1Anti-α-Actinin, clone EA-53, dilution 1:800). Preference was given to monoclonal antibodies. However, in cases where monoclonal was not available, polyclonal antibodies were used.

Secondary fluorescent Antibodies used in this study were: Invitrogen AlexaFluor 568 Goat Anti-Mouse IgG (H+L); Invitrogen AlexaFluor 488 Goat Anti-Mouse IgG (H+L); Invitrogen AlexaFluor 488 Goat Anti-Rabbit IgG (H+L).

6- Live Pcell Calcium Dynamics Imaging

For Ca^{2+}-specific fluorescence imaging, live Pcells were loaded with Fluo-4AM (Invitrogen FI4210). Fluo-4AM was reconstituted in anhydrous DMSO. Fluo-4 exhibits an increase in fluorescence intensity on binding to Ca^{2+}, with no spectral shift. For these experiments, a stock solution was made using a 1:1 dilution factor (50 μg of Fluo-4AM ester with 50 μL of DMSO). From this, 10 μL Fluo-4 stock solution was added to 1mL cell solution (500 μL cell solution and 500 μL of 500 μM Ca^{2+} Tyrode). This was protected from the light and kept at 25°C for 25 min. Experiments were performed at 25°C and not 37°C to slow the rate of metabolism and degradative processes within the freshly isolated Pcells. Jaffe reports that a 10°C increase in experimental conditions increases the Q10s of a variety of tissues by 2.7 fold (*Jaffe, 2002*). Therefore, by slowing these enzymatic processes we were able to maintain live cells for a longer time.

Following this, cells were loaded into a perfusion chamber on the stage of an inverted 2D microscope, and left in the dark for 5 minutes, allowing them time to settle and cling to the slightly positively charged poly-L-lysine coated perfusion chamber. Cells were perfused with 1mM Ca^{2+}-Tyrode for a minimum of 10 minutes to allow for any remaining dye or metabolites to be washed away. Following this, cells could be examined at higher Ca^{2+} concentrations, depending on the intent of the experiment. To do this, the cells were perfused at 2mM Ca^{2+}-Tyrode for a minimum of 10 minutes, and then this could be repeated with 4mM, and then 8mM Ca^{2+}, as necessary.

Cells were examined using a 2D spinning disc confocal microscope (custom built) with Olympus inverted microscope IX81, CSU-X1 Yokogawa spinning disc, FitC low level intensity fast camera and MAG Biosystems Frap3D lasers.

Spatial and temporal characteristics of local Ca^{2+}-events were measured in Pcell isolates and aggregates using this 2D confocal microscope. Intracellular Ca^{2+}-concentration and events were measured from the fluorescence of the Ca^{2+}-indicator Fluo-4AM. The intensity of the Ca^{2+}-related fluorescence was captured on the FitC low level intensity fast camera. The system was attached to the video port of an inverted microscope equipped with a 60X oil objective lens. Fluorescence images were captured at 30-33 frames/second.

7- Electrical Stimulation of Pcell Aggregate

Action potentials in isolated Pcells and aggregates were evoked with field stimulation. This was carried out to examine the variations in internal Ca^{2+}-dynamics using specific fluorescence from Fluo-4, concomitant with transmembrane voltage

changes. Preparations were excited with square voltage pulses of current at a duration of 20-40ms, at an amplitude 10% above the threshold of activation.

8- Analysis of Spontaneous Ca^{2+} Transients in Porcine Pcells

Qualitative Analysis: Time Course and Spatial Course Measurements of Ca^{2+} Sparks

Typical Ca^{2+} sparks from the SubSL and core regions were analyzed using MAG Biosystems software Region Measurements application to examine their time course, and virtual Linescan application to examine their spatial course. These measurements were taken after a ratio for pixel-to-pixel variations (F/F_o) images was determined. From the time course measurements, we determined Amplitude (F/F_o), Time to Rise (T_{Rise}) and Time to Half Relaxation ($T_{1/2R}$) (Fig. 5). Amplitude is the maximal intensity (F/F_o) of the Ca^{2+}-transient. T_{Rise} corresponds to the amount of time taken from initiation to maximal intensity of the Ca^{2+}-event; while $T_{1/2Relaxation}$ corresponds to the reuptake function in the SR. From the spatial course measurements, we determined Amplitude (F/F_o) and Full Width Half Max (FWHM) (Fig.6). FWHM refers to the spatial distribution of the Ca^{2+}-event, and is reported in microns.

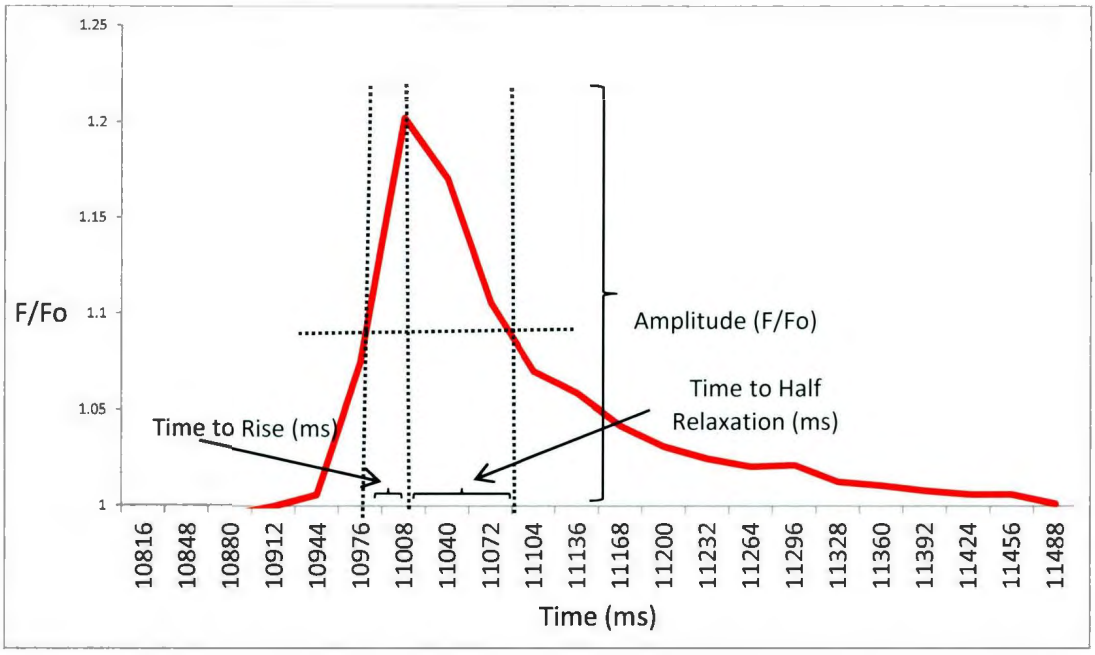

Figure 5: Output from MAG Biosystems software in time course measurements in the analysis of a typical large Ca^{2+}-spark. Measurement parameters shown.

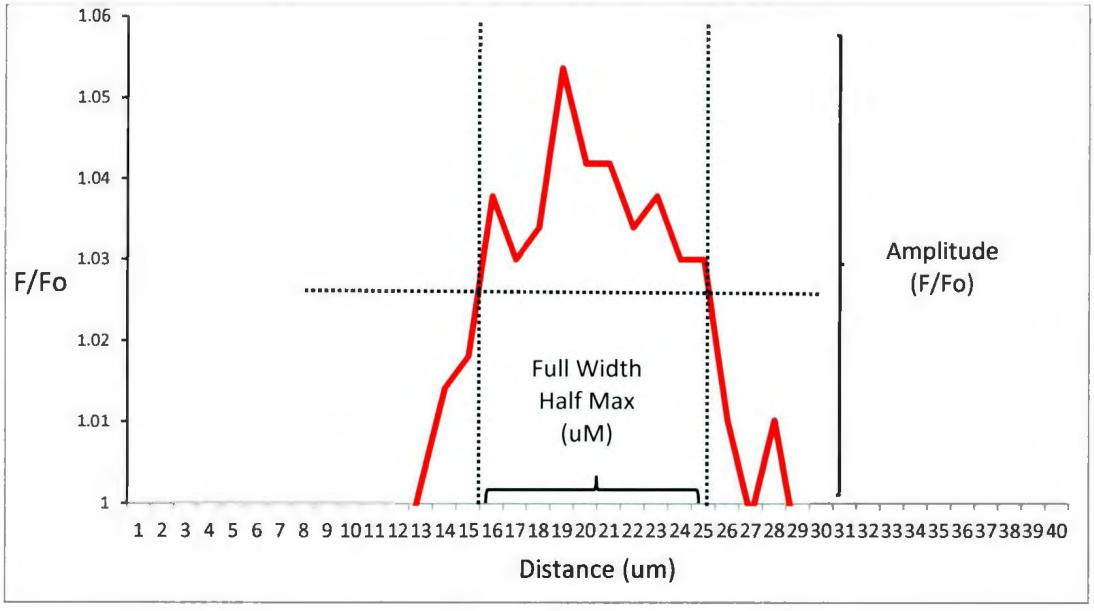

Figure 6: Output from MAG Biosystems software in spatial course measurements in the analysis of a typical large Ca^{2+}-spark. Measurement parameters shown.

Expression of Ca^{2+}-concentration: the Ratio Images

Fluctuations of cytosolic Ca^{2+} are presented as ratio images. This process was to account for inhomogeneities in fluorescence due to the variances in the volume of porcine Pcells. By expressing these values as F/F_0 ratios, investigators ensure that variations in fluorescence reported were actually due to intracellular Ca^{2+}, rather than the size of the cell being examined.

To calculate ratio values, a reference (F_0) image was chosen; this Pcell had a resting amount of Ca^{2+} and was selected just before appearance of the Ca^{2+} transient to be studied. All other frames from the acquisition are divided (pixel by pixel) by F_0 (Fig. 7). This yields the ratio image, which would be used in analyzing the characteristics (in time and space) of Ca^{2+}-transients.

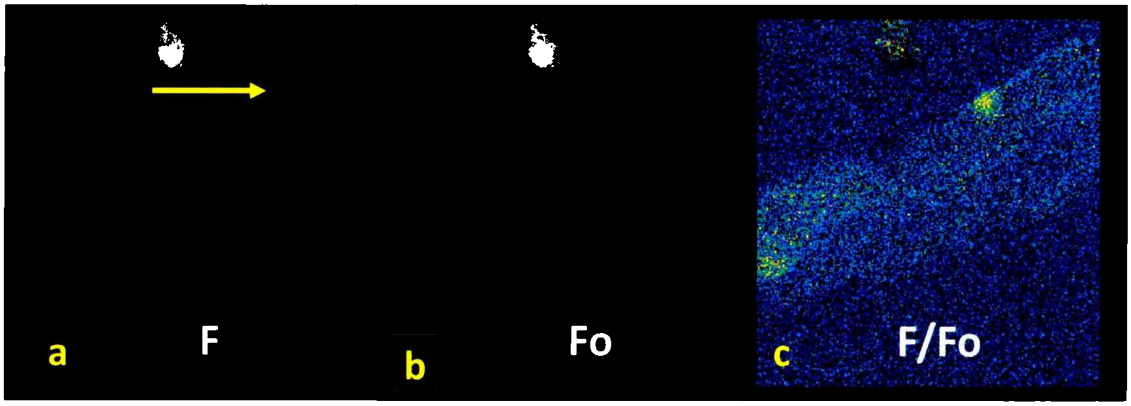

Figure 7: a) F Image: instantaneous fluorescence; Pcell aggregate with a large Ca^{2+} spark indicated by the yellow arrow. b) F_0: Reference fluorescence, resting amount of Ca^{2+}, c) Ratio image (F/F_0). *(Source: December 17 (4mM Ca^{2+}) 7)*

9- Pharmacological Agents and SR-Ca^{2+} Release

Isolated Pcell aggregates were immersed in pharmacological agents which specifically modulated SR Ca^{2+}-proteins. To conduct these experiments, Pcells were examined in spontaneous and electrically evoked conditions. These live Pcells were loaded with Fluo-4, so that Ca^{2+} could be imaged by the 2D Yokogawa spinning disc confocal microscope.

To accomplish this, a 1mL aliquot of the pharmacological agent (agents and concentrations outlined below) was applied directly to the cell suspension in the perfusion bath on the microscope stage. Cell Ca^{2+} dynamics were recorded in the presence of the agent for 2-5minutes, and then the agent was washed out with (2 or 4mM Ca^{2+}) Tyrode solution. Following this washout, cells were recorded for changes in Ca^{2+} dynamics.

Intracellular Ca^{2+}-transients were measured from the fluorescence of the Ca^{2+} indicator Fluo-4. The intensity of the Ca^{2+} related fluorescence was captured from a FitC low level intensity fast camera. The system was attached to the video port of an inverted microscope equipped with a 60X and 100X oil objective lens. Fluorescence images were captured at 30-33 frames/second. Ca^{2+} variations were examined from the pixel-to-pixel ratio F/F_o (where F is the intensity of instantaneous fluorescence, and F_o is the intensity of reference fluorescence). Images were analyzed using MAG Biosystems software.

Pharmacological Agent	Source	Action	Concentration
Dantrolene sodium salt; $C_{14}H_9N_4NaO_5$	Sigma, D9175	Inhibition of RyR_3 *(Zhou et al. 2001)*	1-10 μM *(Davidenko J et al., 1986; Zhou et al., 2001)*
IP_3/BM; rac-myo-Inositol 1, 4, 5-triphosphate hexakis (acetoxymethyl) ester; $C_{24}H_{39}O_{27}P_3$	Sinova, SL-0213	Activation of IP_3 production (*Sinova*)	10 μM *(Lou et al. 2006)*
2APB; 2-Aminoethyl Di-phenyl-borinate; $C_{14}H_{16}BNO$	Sigma, D9754	Antagonist of IP_3R (*Sigma*)	3 μM *(Stuyvers et al. 2005).*
Xestospongin C; $C_{28}H_{50}N_2O_2$	Sigma, X2628	Antagonist of IP_3 (*Sigma*)	10-100 μM *(Contreas-Ferrat et al. 2010; Peters SC and Piper HM. 2007; Kumar et al. 2007)*
Ryanodine; $C_{25}H_{35}NO_9$	Ascent Scientific, Asc-083	Antagonist of RyR *(Cordiero et al. 2001)*	10 μM *(Baéz-Ruiz and Diaz-Muńoz, 2011)*

Table 1: Description of pharmacological agents used in the modulation of SR Ca^{2+}-channels in porcine Pcells.

10-Statistical Analysis

Stochastic data which exhibited a non-Gaussian distribution are represented in the form of histograms. Figure 22 presents distribution histograms to describe the principal characteristics of the Ca^{2+}-transients. Fifty Ca^{2+}-transients of each type were examined (SubSL sparks, core sparks, wavelet and CWW), from 7 porcine hearts. Here Microsoft Excel was used to create these plots. In Fig 22a the bin size was 0.01 F/Fo, beginning at

1.01 F/Fo. In Fig 22b, the bin size was 15ms, beginning at 0ms. In Fig 22c, the bin size was 15ms, beginning at 0ms. In Fig 22d, the bin size was 0.01 F/Fo, beginning at 1.01 F/Fo. In Fig 22e, the bin size was 5μm, beginning at 10μm.

Simple linear regression was used to examine the relationship between a normally distributed dependent variable, and one or more continuous independent (predictor) variables (Forthofer et al. 2007). There are several assumptions which must be made before using regression analysis on the data: the data must fit a Gaussian distribution, Y values must be independent of one another, and the observations must be from a random sample of the test population (Dawson and Trapp, 2001). Linear regression was used in Fig. 25 and 26 to describe the changes in Ca^{2+}-event rates with increasing external [Ca^{2+}] and Fig. 28, to describe the relationship between Time to Half relaxation of Wavelets and external [Ca^{2+}] (1, 2, 4 and 8mM) (N=31 Pcells).

Correlation coefficients (R^2) close to 1 show that the data can be statistically 'explained' by a linear relationship (see Figs. 25, 26 and 28).

The Analysis of Variance (ANOVA) test can be used to test the hypothesis that the means of two or more groups are equal. These groups must be normally distributed (NIST/SEMATECH, 2012). Fig 25 (N=61 Pcells) presents a comparison of event rates of SubSL and core sparks, with varying external Ca^{2+}-concentrations (1, 2, 4 and 8mM). These means were analyzed using ANOVA to look for statistical significance. Other data analyzed with ANOVA are presented in Fig. 26 (N=61 Pcells), 27 (N=19 Pcells), 29

(N=13 Pcells) and 30 (N=10 Pcells). Student's T-tests are used in descriptive statistics, to help investigators describe and summarize data (Dawson and Trapp, 2001). Student's T-tests were used in the investigations presented in Fig. 32 (N=5 Pcells) and 33 (N=7 Pcells).

When using probability tests such as ANOVA and T-tests, a level of significance (p-value) has to be set. In this study, the p-value was set at 0.05, 0.01 or 0.001. The level of significance gave the probability of incorrectly rejecting the null hypothesis when it was actually true. This probability was therefore, set as small as possible (Dawson and Trapp, 2001). Within this thesis, P-values were reported in Fig. 25, 26, 27, 29, 30, 31, 32 and 33.

Results

1- Isolated Pcells and Aggregates

Single Pcells often had a characteristic 'wavy' appearance, as seen in light microscopy (Fig. 8a). Pcells in aggregates (Fig. 8b) were long and slender, maintaining a cylindrical shape when connected end-to-end in the strand. Like myocytes, Pcells were striated. These cells did not have the staircase-like cell ends that were seen in ventricular myocytes (Fig. 9b, 10); rather they had finger-like projections at each end. Isolated Pcells had smooth edges and membranes that were bleb- and granule- free.

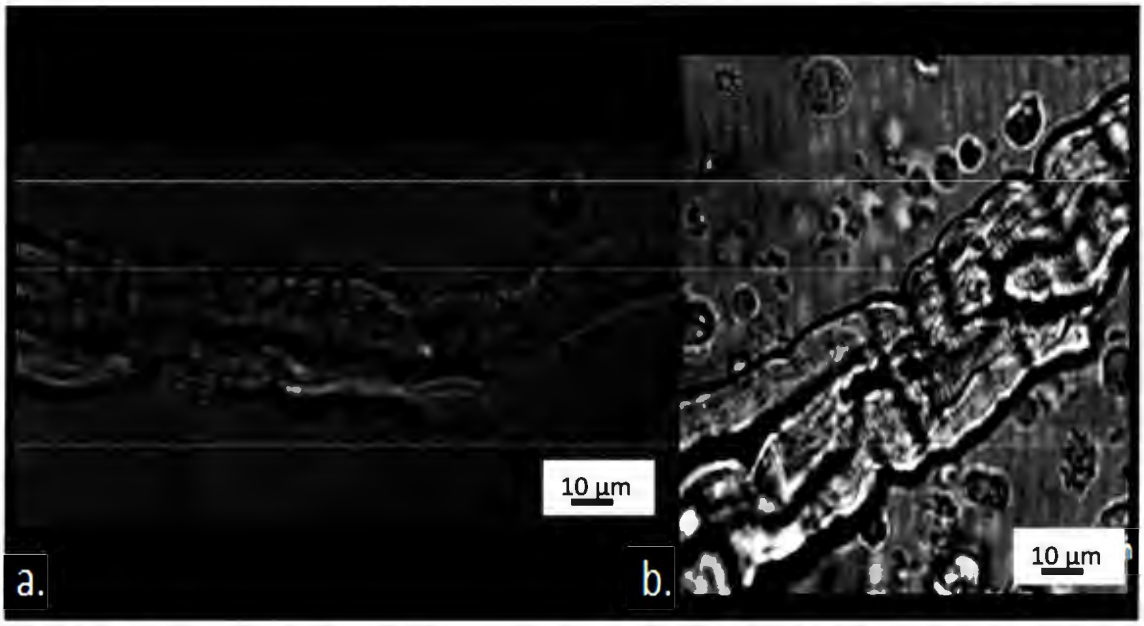

Figure 8: a) White light focused image of a single Pcell. Cell is striated, and the plasma membrane is granule and bleb-free. Cell ends are long and finger-like, while the cell is long and thin. b) Isolated Pcell aggregate. Cells are long and thin, with striations and smooth membrane. *(Source: a) Dec 18-Acquired Images-wholegoodPcell; b) Dec 18-Acquired Images-BFPcellaggregate)*

2- Characterization of the Sarcomeres: Immunofluorescence of Alpha-Actinin

Immunofluorescence studies localizing sarcomeric protein α-actinin were used in porcine cardiomyocytes (Fig.10a, b) to characterize myofibrils. This study showed that α-actinin was present in a 2μm striated pattern throughout the cell and showed a uniform distribution of the myofibrils throughout the cell, which was comparable to actinin-striation detected in the well-known model of ventricular myocytes (Fig.9). Alpha-actinin indicated an average sarcomere length of 2μm and showed a uniform distribution of the myofibrils throughout the cell. This suggested a comparable myofibril arrangement in Pcells and myocytes. The 2μm striation indicated that sarcomeres were in a relaxed state and the cells were not Ca^{2+} overloaded.

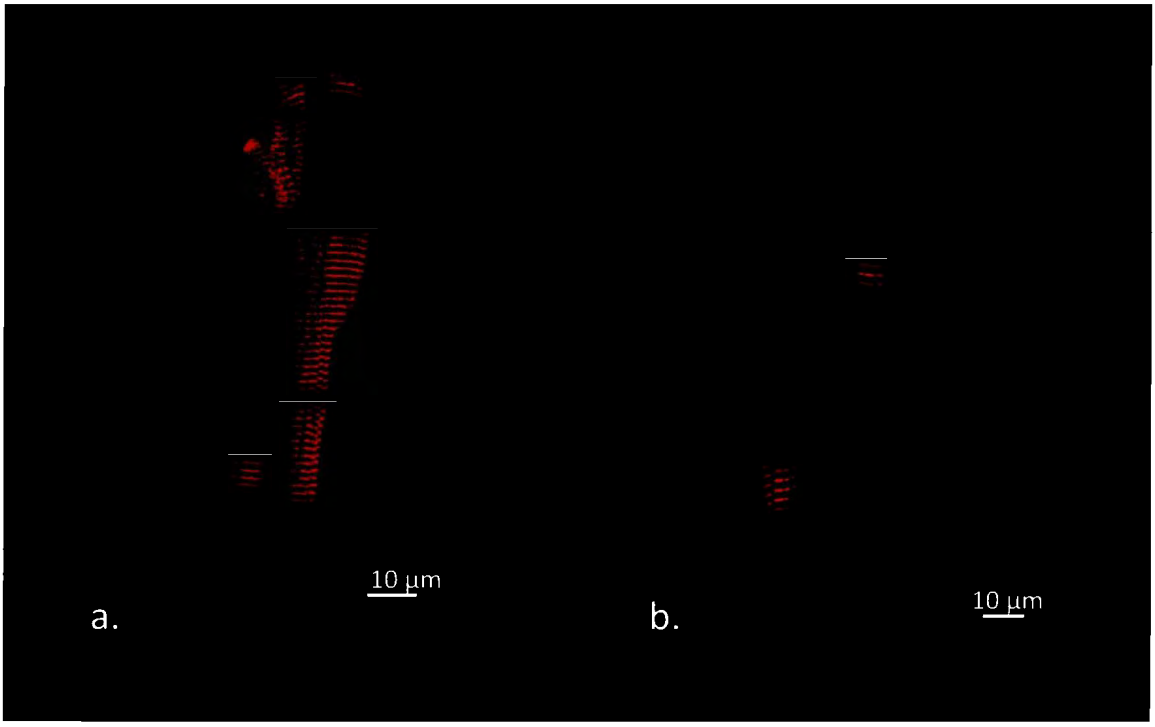

Figure 92: Rat ventricular myocyte after undergoing immunofluorescence specific for α-actinin, shows fluorescence in a striated pattern throughout the cell. *(Source: a) Dec 23-8a, b) Dec 23-17a)*

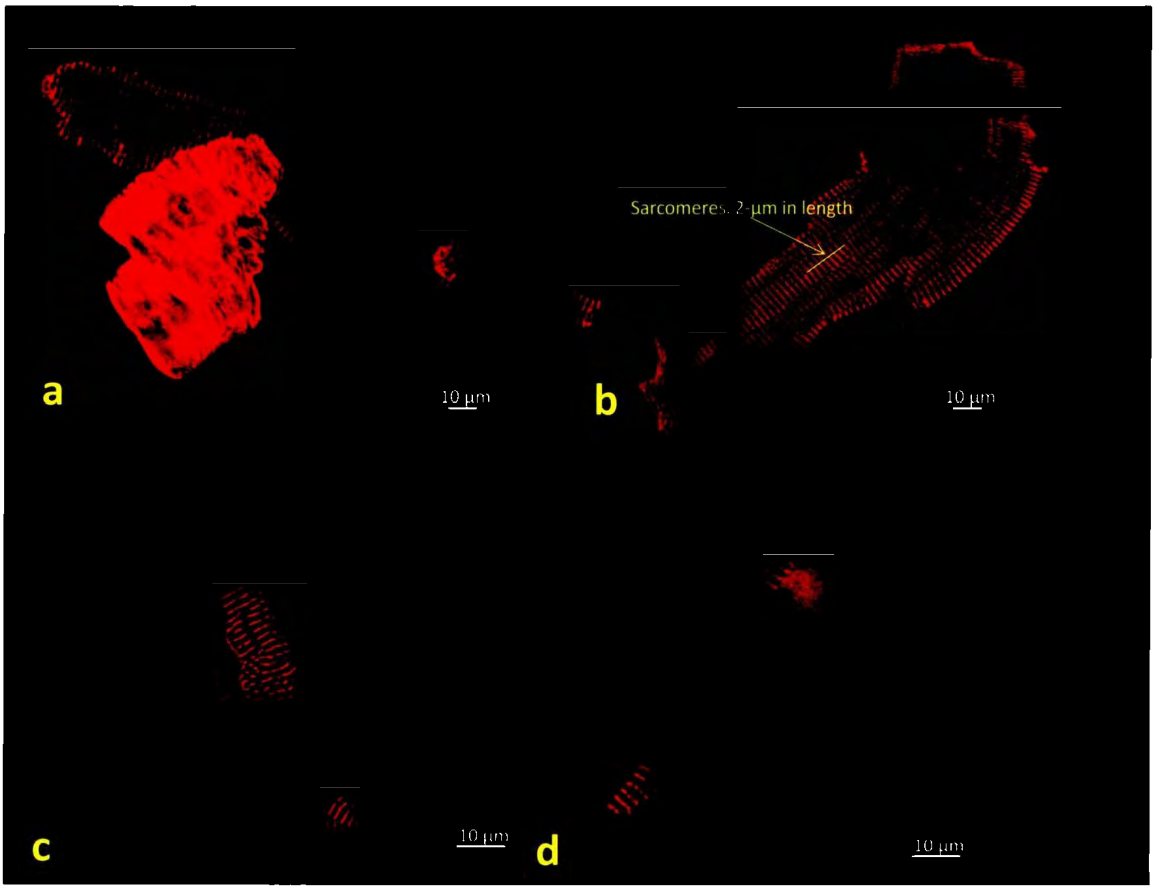

Figure 10: Alpha-actinin localization in porcine cardiac tissue. Sarcomere lengths were 2µm, observed throughout the Pcells: a) Pcell, note the striations *(Source: December 3-12b);* b) Ventricular myocyte, note the striations *(Source: Dec 3-15b);* c and d) further examples of Pcells *(Source: Dec 3-16b (c) and 8c (d)).*

3- Characterization of Sarcolemma by Di-8-ANEPPs

To detect T tubules (see *Background* section), we stained the sarcolemma of Pcells using the membrane specific, voltage sensitive fluorescent dye Di-8-ANEPPs. We then compared these results with those obtained from ventricular myocytes (Fig. 11b), which were known to have a well-developed T-tubule system. Stained with Di-8-ANEPPs, Pcells did not show the typical striations observed in myocytes under the same conditions (Fig. 11a) as myocytes. The same observation was made in Pcells isolates, as in large

aggregates of 2-10 Pcells (Fig. 11c). The finding that no striated pattern was seen in porcine Pcells indicated that these cells did not contain a T-tubular network.

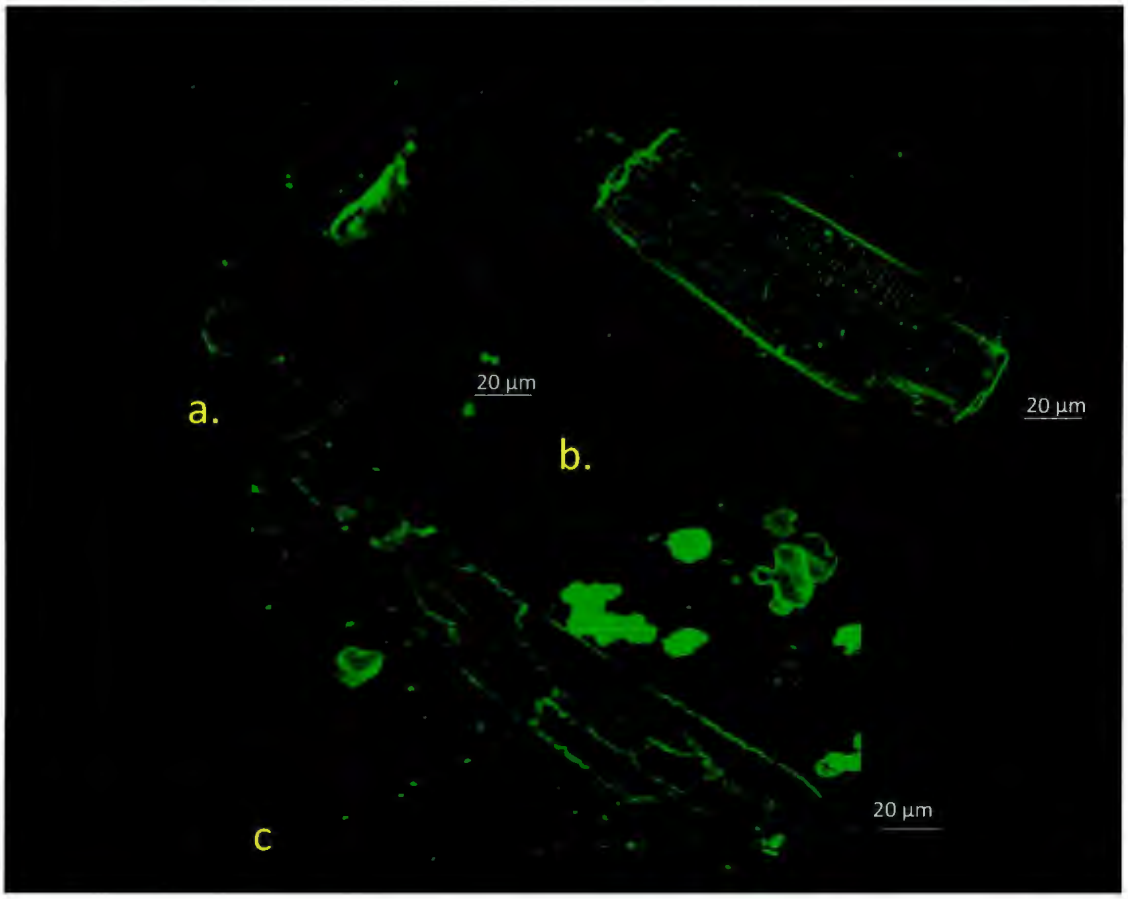

Figure 11: (a) Isolated Porcine Pcells (aggregate of 2) stained with Di-8-ANEPPs. Note that the sarcolemmal dye is only seen around the periphery of the cell, indicating that there are no infoldings of the membrane, indicative of the lack of a T-tubular system. (b) Porcine ventricular myocyte stained with Di-8-ANEPPs. Note that the sarcolemmal dye is found in a striated pattern inside of the cell, indicating that this cell contains an extensive T-tubular system. c) Isolated porcine Pcell aggregate, dyed with Di-8-ANEPPS, examined using scanning laser confocal microscopy. Cells adhere to one another tightly end-to-end. *(Source; a) Feb 14-Pcell3; b) June 10-2b; c) January 8-Pcell14)*

4- Examination of Pcells by Electron Microscopy

EM images of Pcells (Fig. 12, 13) showed abundant myofibrils regularly aligned in the longitudinal direction with a high density of mitochondria in the inter-myofibril space (arrows in Fig. 12). In the myocardium *(Di Miao et al., 2007a,b)*, the T-tubules are arranged in the transverse plane of the cell, as opposed to myofibrils which are longitudinal. This makes T-tubules appear as small "holes" at the level of the Z-lines of the sarcomeres. In porcine Pcells, these "holes" were not found (Fig. 12, 13), which was supportive evidence, at the ultrastructural level, for the absence of T-tubules in Pcells.

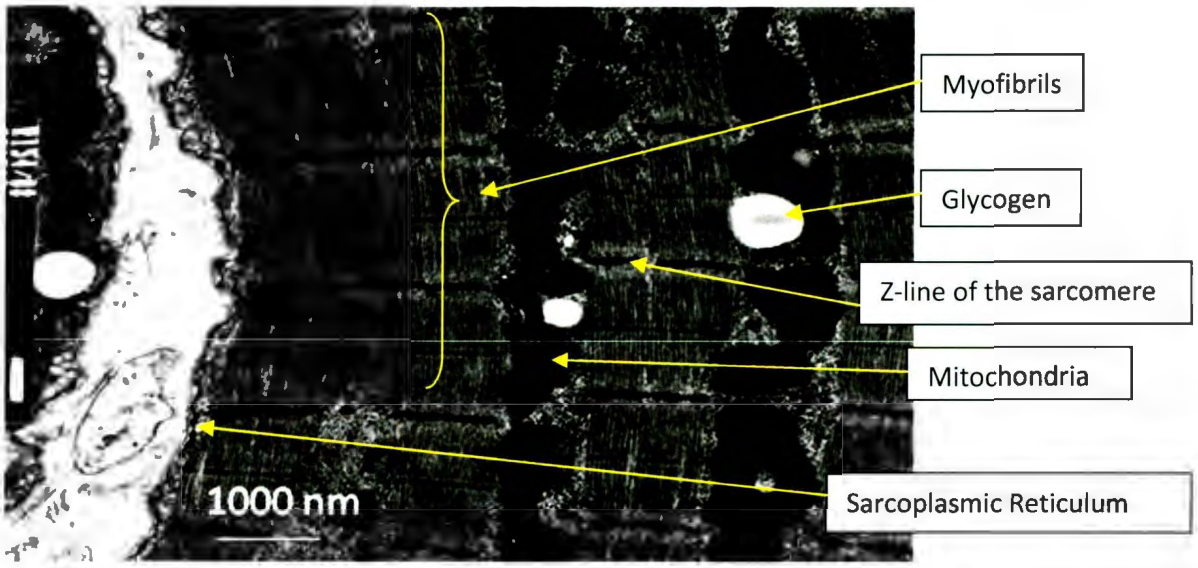

Figure 12: Electron Microscopy of a porcine Purkinje Strand. Note that there are many myofibrils, abundant mitochondria, sarcoplasmic reticulum and a fair amount of glycogen visualized. *(Source: Pig Purkinje EM Pics-R154-08-081595X10K)*

Figure 13: Electron microscopy images of the porcine Purkinje-strand. Note the many ordered myofibrils, mitochondria, SR and glycogen (see Fig. 13 for image guide). *(Source: Pig Purkinje EM Pics-R184-08-(left) 081655X10K, (centre) 081656X10K, (right) 081661X10K)*

5- The Triple Layered System of Ca^{2+}-Activation in the Porcine Pcell

A-Components of the Centripetal Activation model in porcine Pcells

A.1. Non-isoform selective staining for RyRs

Staining for all RyR isoforms with a fluorescent anti-RyR (non-isoform selective) antibody showed fluorescence with striated distribution throughout the Pcells (Fig. 14). We found that the antibody distribution showed striations with a 2μm period, matching the sarcomere length pattern of resting Pcells (as seen in Fig. 10a, 10b).

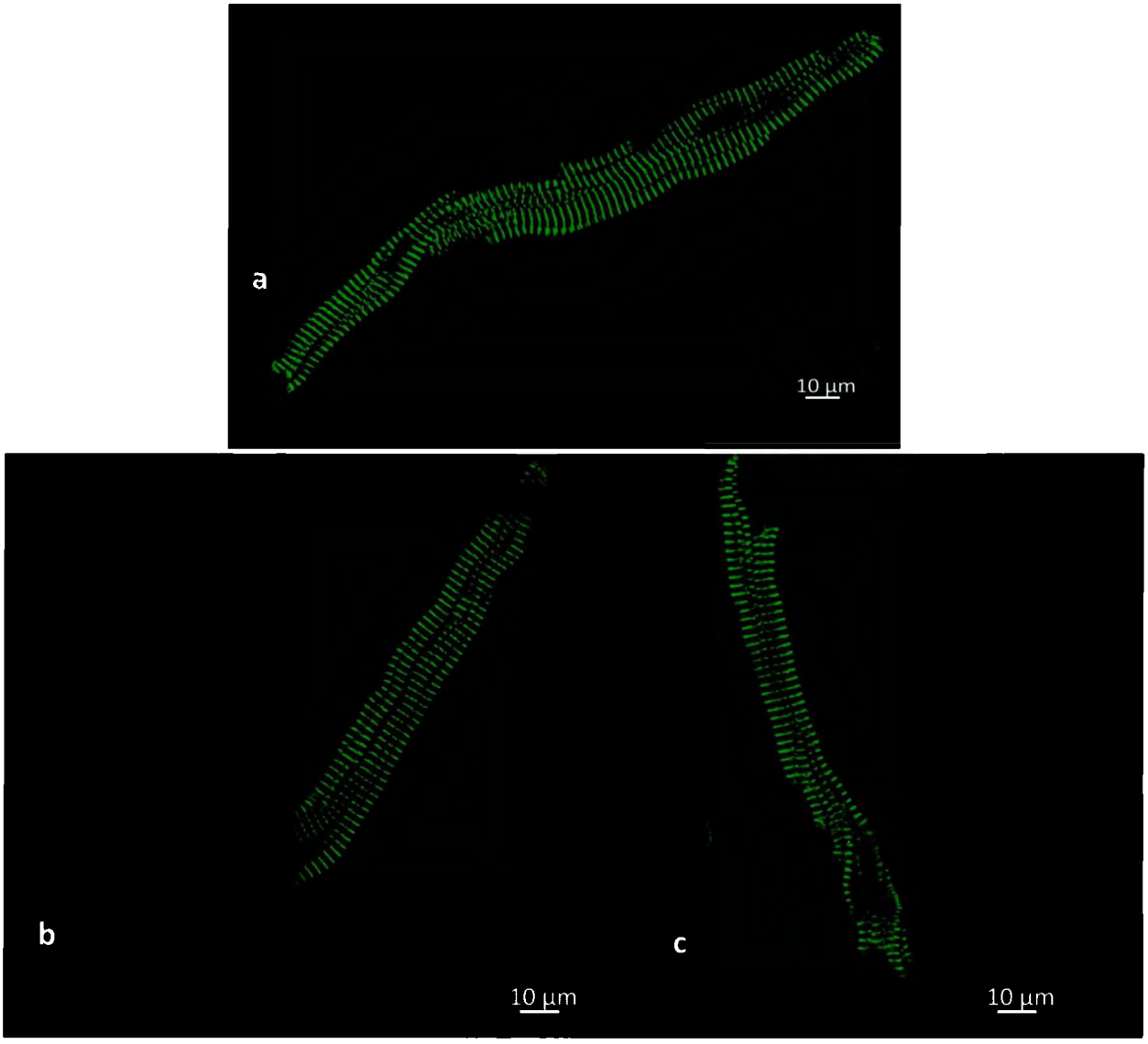

Figure 14: RyR Immunofluorescence in porcine Pcells. Pcells displayed striated fluorescence throughout, in 2µm intervals. These striations corresponded to the z-disc of the sarcomere, with the exception of the nuclei which didn't contain RyR (Source: December 19-7a); b and c) Further results of RyR Immunofluorescence, striations were found throughout the Pcell, with the exception of the nuclei. *(Source: December 19-11a (b) and 14a (c))*

A.2. Specific staining for RyR_3

Immunofluorescence specific for RyR_3 showed a signal exclusively at the periphery of the cell: the SubSL region (Fig. 15, 16). This fluorescence appeared in

striations and did not enter the core of the cell, as shown by the Z-stack images of Fig. 16.

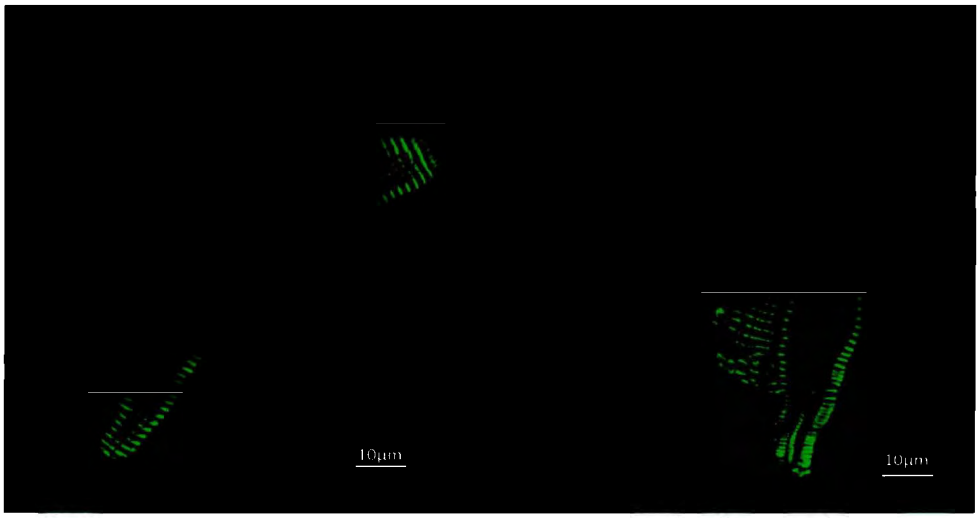

Figure 15: RyR_3 immunofluorescence of porcine Pcells. Pcells displayed fluorescence only in the peripheral SR of the cylindrical shaped cell, extending approximately 4-6μm inwards from the plasma membrane. These images were taken as serial longitudinal optical slices, using 2D confocal microscopy.

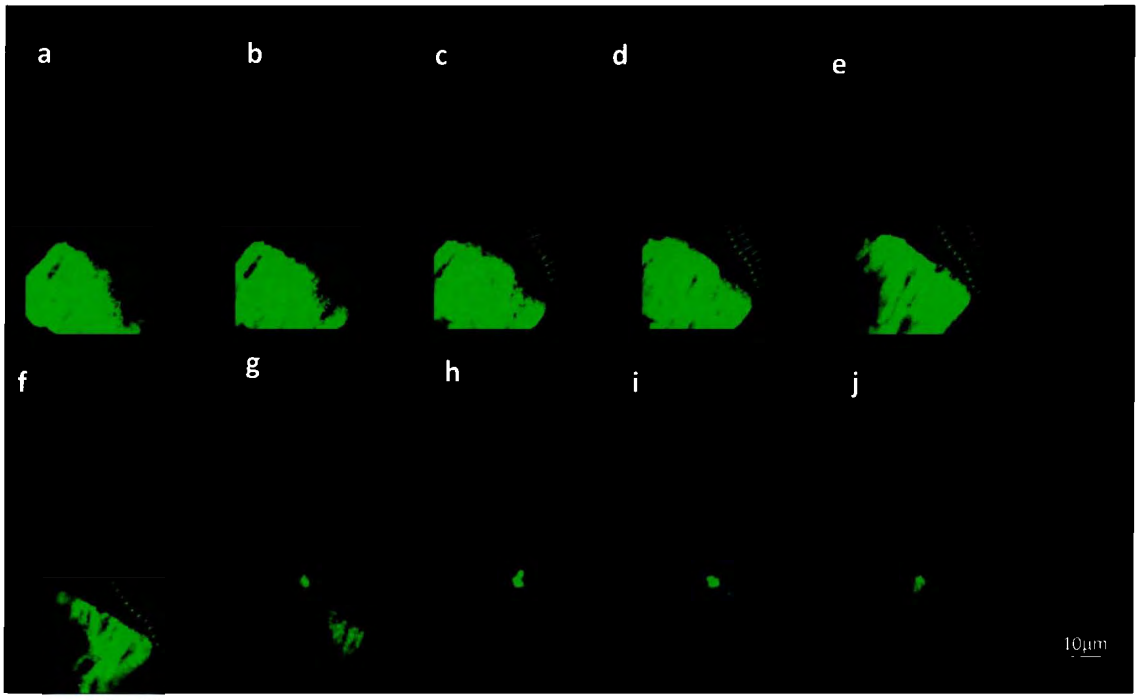

Figure 16: RyR_3 immunofluorescence of porcine Pcells. Pcells exhibited fluorescence only in the peripheral SR of the cylindrical shaped cells. Z stack images revealed fluorescence localized specifically in a restricted region, just inside of the sarcolemma. This series of images was taken using 2D scanning laser confocal microscopy techniques as a serial stack of longitudinal optical slices. Image (a) was the bottom of the cylindrically shaped cell. Images (b-i) were taken in 5-10µm intervals moving towards and through the core of the cell. Image (j) was taken at the top of the cell.

A.3. Specific staining for IP_3R

Specific fluorescent antibody anti-IP_3R_1 was used to localize this SR protein. The results showed that IP_3R_1 was expressed on the inner face of the sarcolemma of porcine Pcells. IP_3R_1 is also densely located in the nuclear regions of the porcine Pcells (Fig.17).

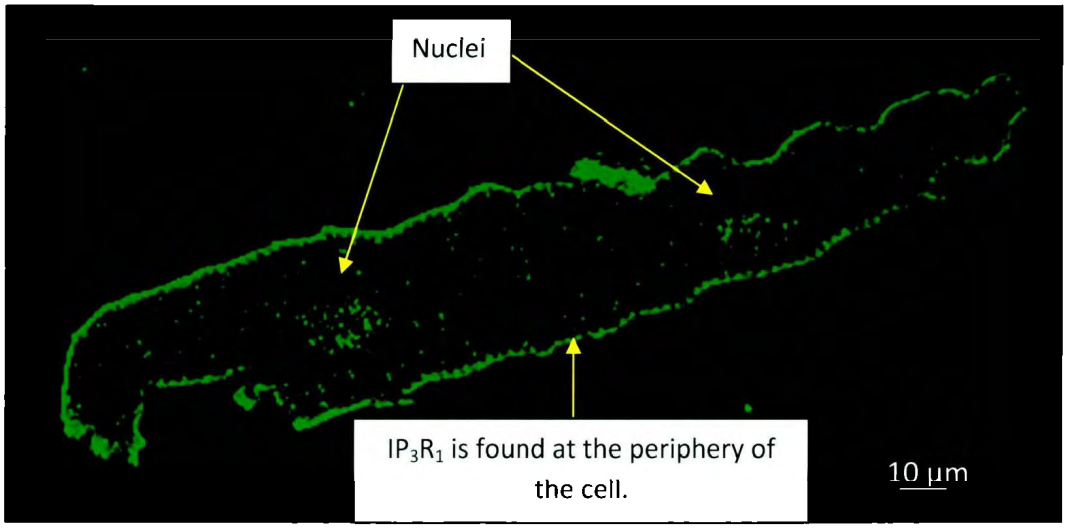

Figure 17: IP_3R_1 immunofluorescence of porcine Pcells. Pcells displayed IP_3R_1 in the peripheral SR, just inside of the SR (the NearSL) approximately 1.7-2µm in width, and surrounding the nuclear regions (arrows). *(Source: May 13-28 zstep-024)*

A.4. Specific staining for RyR_2

Specific immunostaining of RyR_2 (Fig. 18) in porcine Pcells revealed a lack of fluorescence in a region matching approximately the distribution of RyR_3s (see above, Fig. 15, 16). Consistent with our first isoform non-specific staining of RyR (Fig. 14), RyR_2s were arranged in a striated pattern throughout the cell (Fig. 18).

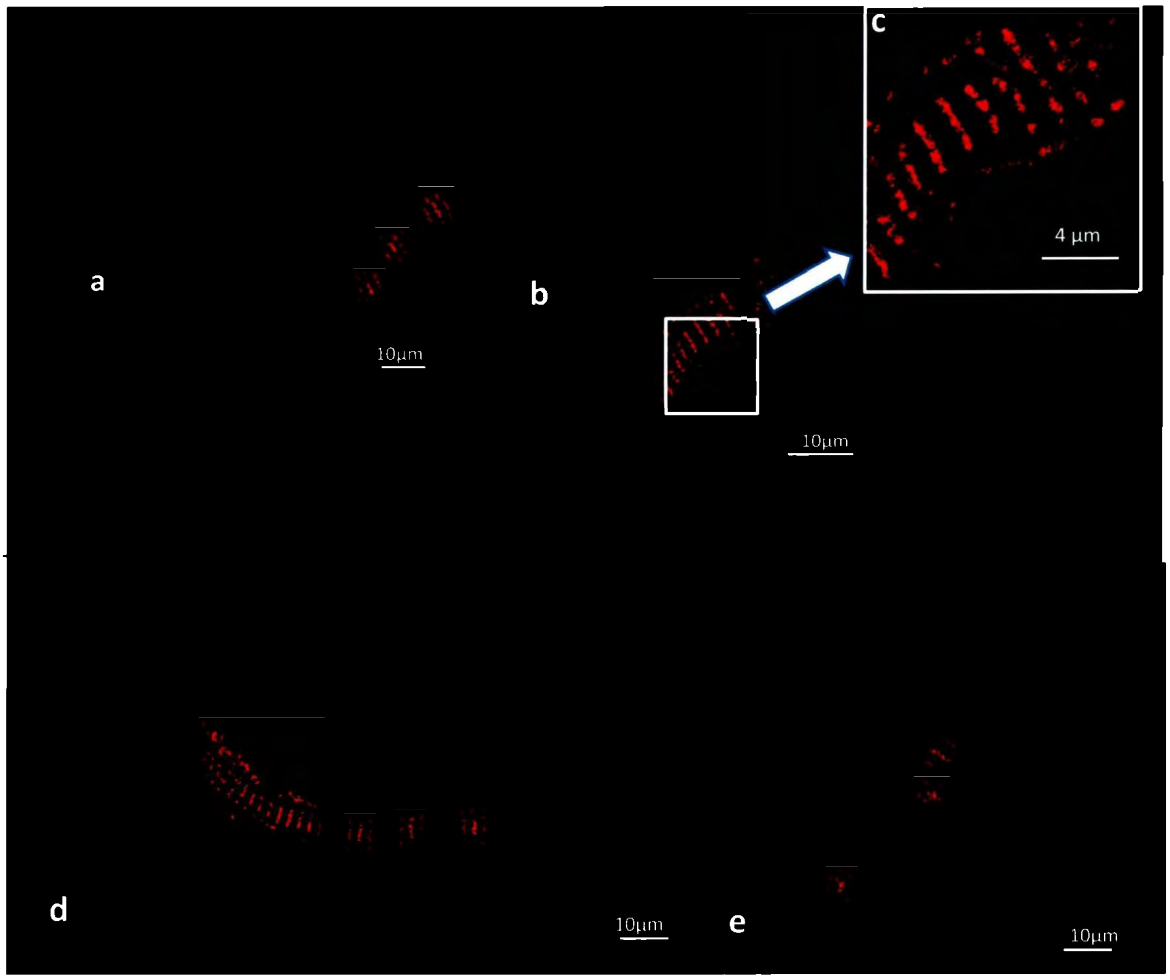

Figure 18: RyR_2 immunofluorescence of porcine Pcells. Note the striations of fluorescence throughout the cell SR, with the exception of an apparent void (2μm-width) just inside of the sarcolemma and within the nuclear region.

B-Does the model of Centripetal Activation work the same way in porcine Pcells?

The currently proposed model of Centripetal Activation in Pcells from large mammalian hearts was described in Fig. 4. In this model, large sparks in the SubSL region activated RyR_3-proteins which created small propagating Ca^{2+}-transients called wavelets. If conditions were different from normal, such as during stimulation or

following an MI, wavelets could activate central RyR_2s leading to large, electrogenic CWWs. This electrogenic activity could perpetuate from cell to cell within an aggregate *(Stuyvers et al., 2005).*

In our study, live porcine Pcells were examined using 2D confocal microscopy (see *Methods*) in order to characterize the Ca^{2+} events generated in the three distinct regions of SR-Ca^{2+} channels. The Ca^{2+}-activity was assessed in electrically stimulated cells ("stimulated conditions"B.1.) and in un-stimulated cells ("spontaneous conditions"B.2.).

B.1. Stimulated Conditions.

When ventricular myocytes were stimulated electrically, they responded with a uniform and synchronous elevation of the cytosolic Ca^{2+}-concentration (see representative example in Fig. 19).

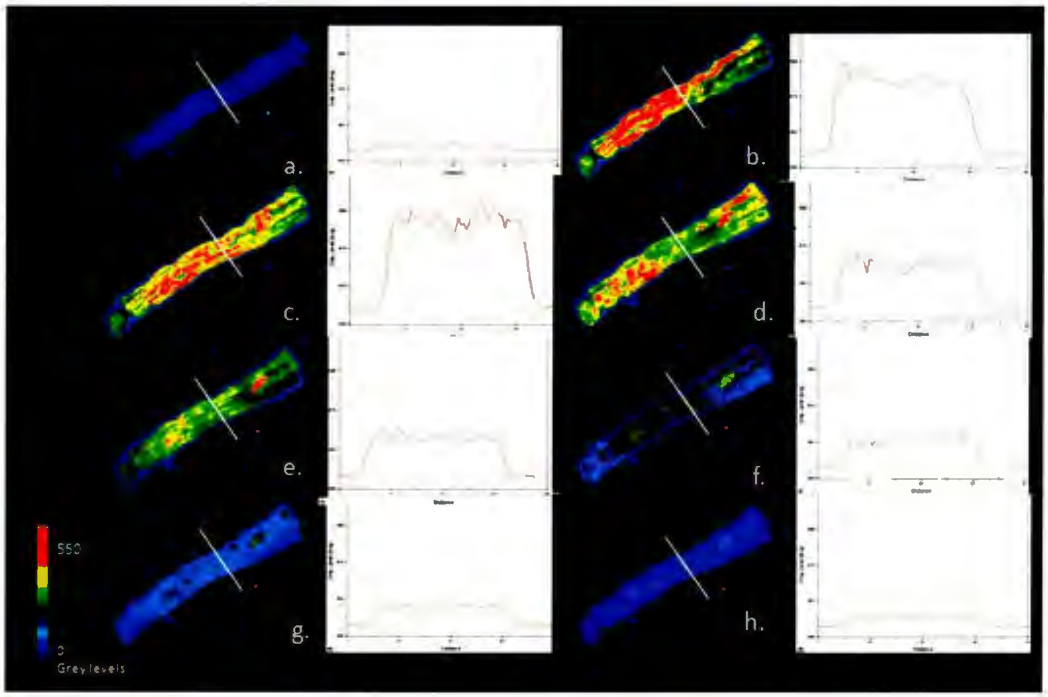

Figure 193: Series of F-Fo frames in time, showing activation of a single porcine cardiac ventricular myocyte after being electrically stimulated with a field stimulus. a) Basal level of intracellular Ca^{2+}; b-e) Immediately upon stimulation, the cell responded with a uniform increase in fluorescence; f-h) Stages of recovery following stimulus, cell returned to baseline fluorescence. Using the Linescan application of the MAG Biosystems Software, intracellular fluorescence was measured and was reported to the right of each image. Above: Fluorescence (pixels) vs. Distance (μm). Intensity of fluorescence was reported in units of pixels. *(Source: Dec 18 (2mM) 8)*

Under the same stimulated conditions, porcine Pcells responded with a peripheral increase of Ca^{2+}-concentration first (see arrows in diagrams of Fig. 20c), followed by a second increase in the cell core (Fig. 20f). The overall Ca^{2+}-elevation exhibited a typical centripetal propagation: from the cell membrane into the cell core.

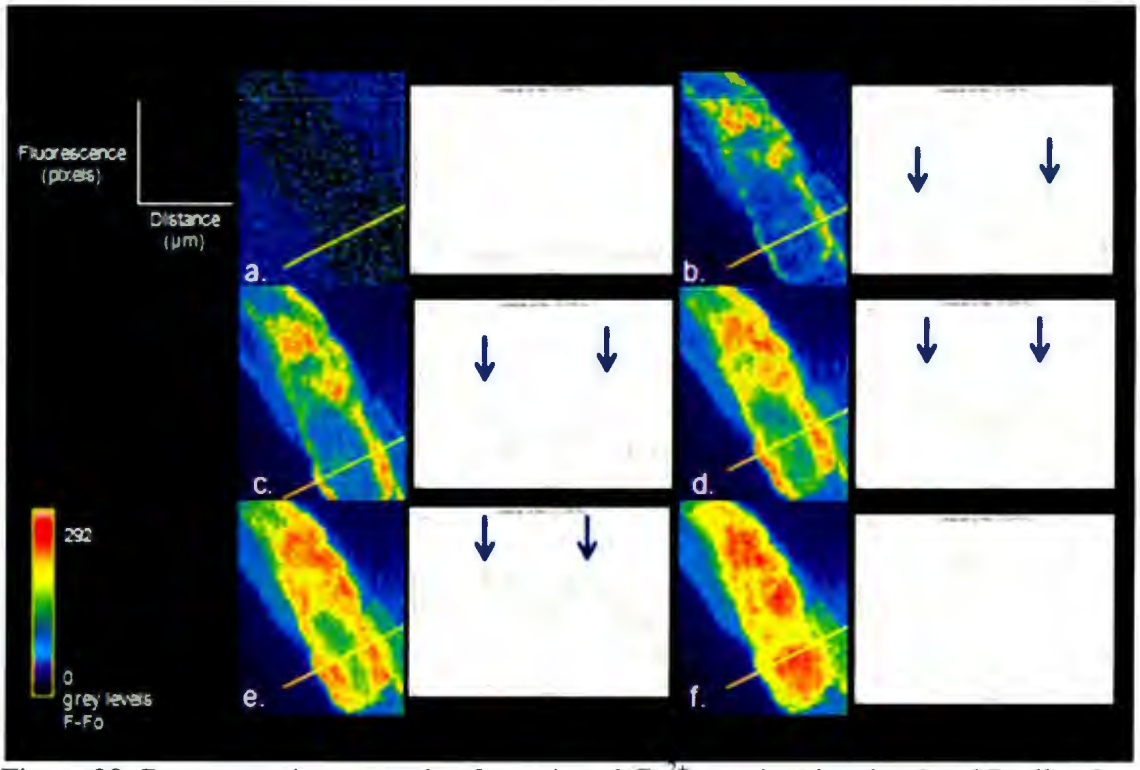

Figure 20: Representative example of centripetal Ca^{2+} transient in stimulated Pcells of swine. Series of frames in time showing the response of one cardiac Pcell aggregate as it was electrically stimulated. The plane of focus was through the core of the top cell in the aggregate. The sarcolemma could be visualized only at the periphery of this cell. (a) The cell was at baseline fluorescence, with very little intracellular Ca^{2+}-activity observed; (b) Immediately after being stimulated, the cellular response was a release of Ca^{2+} only at the level of SR in close apposition with the plasma membrane, followed by (c-f) a massive Ca^{2+}-release at the cell core. *(Source: Nov 27 (4mM) 23)*

B.2. Spontaneous conditions

In cardiac myocytes, small Ca^{2+}-sparks were visualized homogenously throughout the SR of un-stimulated cells. In contrast, within Pcells there were two distinct types of Ca^{2+}-sparks visualized. There were large sparks which occurred in the SubSL region (Fig. 21a), and smaller sparks throughout the cell core (Fig. 21b).

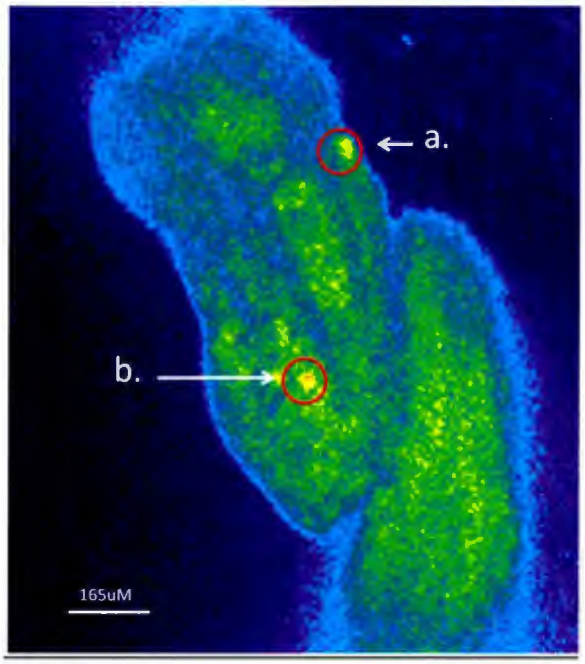

Figure 21: Spontaneous Ca^{2+}-transients visualized in cardiac Pcells. a) SubSL sparks occurred at the periphery of the cell. These were typically much larger than those observed in the core. b) Core sparks occurred throughout the SR of the Pcell, not specifically near the SL. Core sparks were typically smaller than SubSL sparks. This image is part of a Pcell aggregate which has been stained with Fluo-4AM, Ca^{2+}-specific fluorescent dye. *(Source: Nov 27 (4mM) 11)*

C - Functional characterization of the model of Centripetal Ca^{2+} Activation in porcine Pcells

C.1. Analysis of Non-Propagating Spontaneous Ca^{2+}-transients

Spatial and temporal characteristics of local Ca^{2+}-events were measured in single Pcells and Pcell aggregates, as indicated in the *Methods* section. Typical Ca^{2+}-events were analyzed using the Region Measurements application in the MAG Biosystems software; time course and spatial course were measured using virtual linescans. These measurements were implemented from ratio (F/F_o) images. We characterized the time

course of Ca^{2+} events by measuring Amplitude (F/F_o), Time to Rise (T_{Rise}) and Time to Half Relaxation ($T_{1/2R}$) of the Ca^{2+}-transient (Fig. 5).

When Ca^{2+}-sparks were sampled by confocal microscopy, the analysis was done through distribution histograms due to the "out-of-focus" occurrence of some events (see *Methods* section). However, the histograms of Fig. 22 showed that the distribution of data was nearly Gaussian ("Bell shape distribution"). To collect this data we used 2 dimensional confocal microscopy, which reduced the influence of "out-focus" sparks in our measurements, as compared to classical single scanline confocal microscopy. This permitted a normal statistical comparison of the data (see Tables 2 and 3).

Figure 22: Distribution histograms of the Time and Spatial Course Characteristics of SubSL and core sparks, as assessed using 2D confocal microscopy (*full description below*):

a)

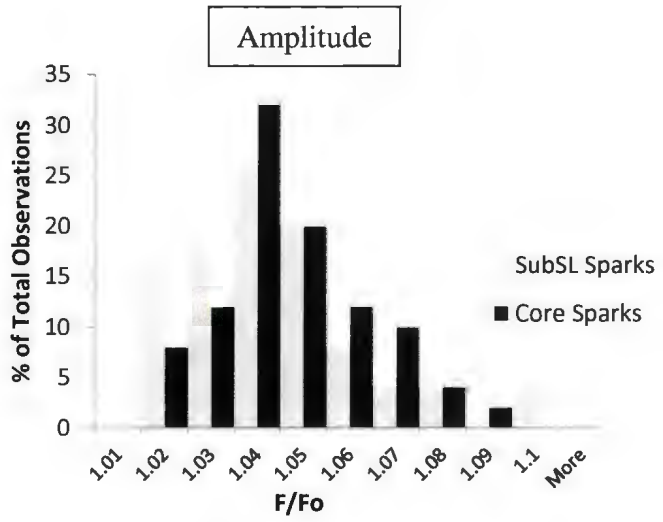

b)

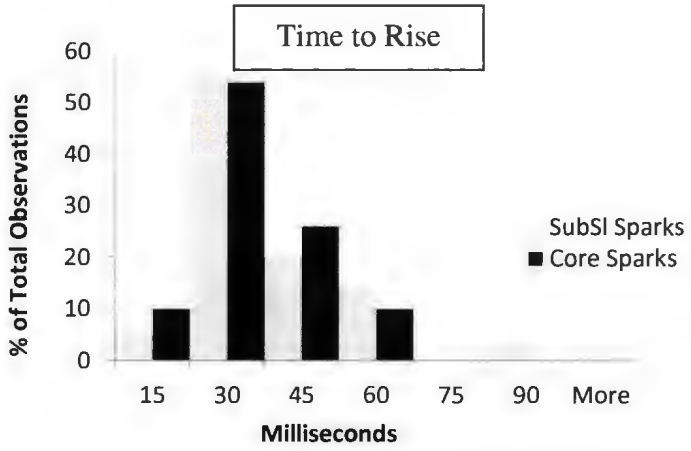

c)

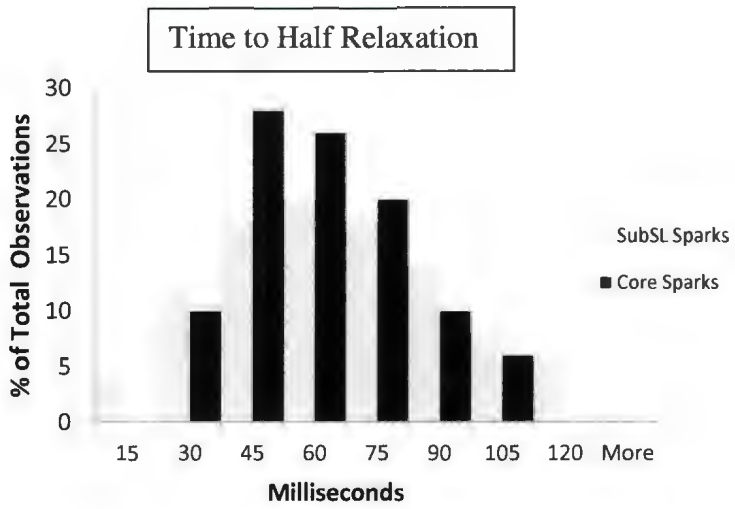
Time to Half Relaxation
% of Total Observations
30
25
20
15
10
5
0
15
30
45
60
75
90
105
120
More
Milliseconds
SubSL Sparks
Core Sparks

d)

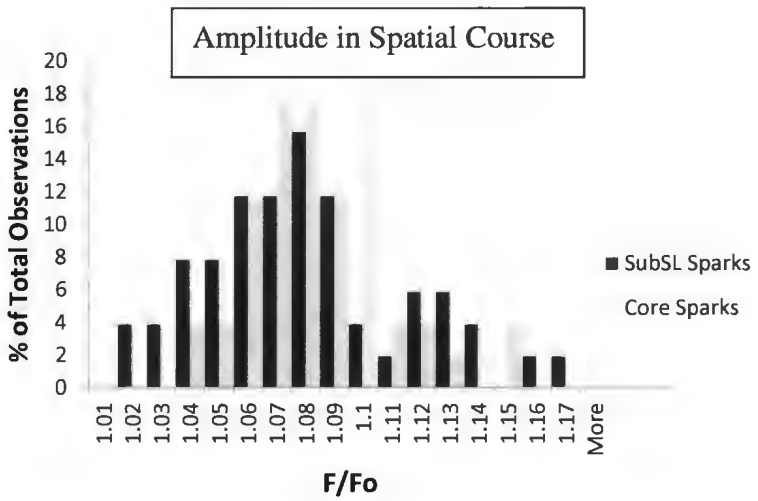
Amplitude in Spatial Course
% of Total Observations
20
18
16
14
12
10
8
6
4
2
0
1.01
1.02
1.03
1.04
1.05
1.06
1.07
1.08
1.09
1.1
1.11
1.12
1.13
1.14
1.15
1.16
1.17
More
F/Fo
SubSL Sparks
Core Sparks

e)

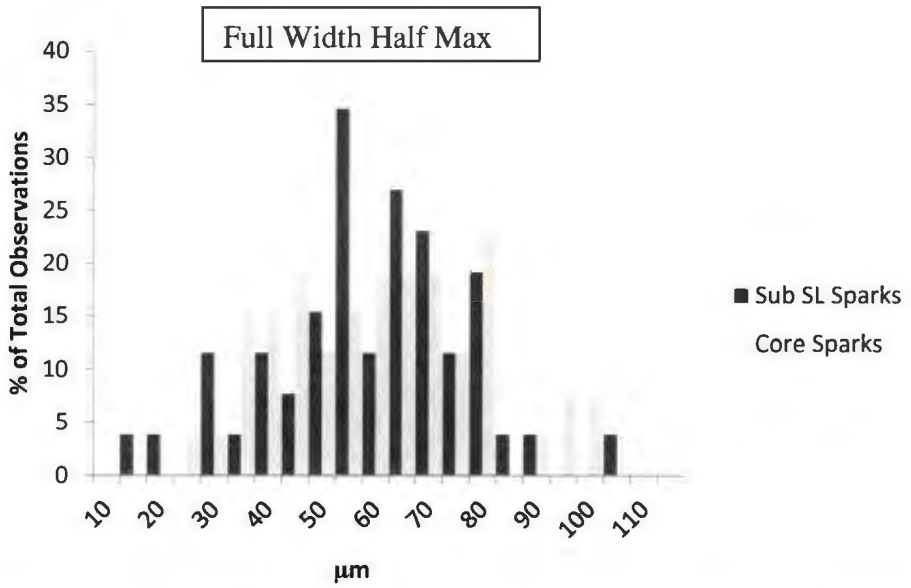

Figure 22: Spatiotemporal characteristics of sparks in the SubSL and core of porcine Pcells, as assessed using 2D confocal microscopy. N=50 SubSL and 50 core sparks, randomly chosen from 7 porcine hearts. a-c) Ca^{2+}-spark time course analysis. a) Distribution histogram of core spark amplitudes (F/F_o). There was no significant difference between spatial course amplitudes of these species of sparks; b) Distribution histogram of SubSL and core spark time to rise (ms). There was no significant difference between these species of sparks; c) Distribution histogram of SubSL and core spark Time to Half Relaxation (ms). There was no significant difference between these species of sparks. d-e) Ca^{2+}-spark spatial course analysis; d) Distribution histogram of SubSL and core spark amplitude in spatial course. There was no significant difference between these species of sparks; e) Distribution histogram of SubSL and core spark full width half max (FWHM; um) in spatial course. There was no significant difference between these species of sparks.

As shown in Fig. 22, no significant differences could be detected in the time course (Fig. 22a, b, c, Table 2) or in the space development (Fig. 22e, f, Table 3) of the Ca^{2+}-sparks within the SubSL and core regions.

	Amplitude (F/Fo)	$T_{Rise(ms)}$	$T_{1/2Relaxation(ms)}$
SubSL Sparks (n=50)	1.0396 ± 0.0028	30.8ms ± 2.4	60.3 ± 3.9
Core Sparks (n=50)	1.0451±0.0029	28.4ms ± 1.8	58.0 ± 3.7

Table 2: Results from the time course analysis of Ca^{2+}-sparks from porcine Pcells. Values showed no statistically significant differences (P>0.05) between core and SubSL sparks. N=50 SubSL and 50 core sparks, randomly chosen from 7 porcine hearts. Values were presented as mean +/- standard error.

	Amplitude (F/Fo)	Full Width Half Max (μm)
SubSL Sparks (n=50)	1.0752ms ± 0.0049	57.0ms ± 2.6
Core Sparks (n=50)	1.0793ms ± 0.0033	56.7ms ± 2.6

Table 3: Results from the analysis of the spatial course of Ca^{2+}-sparks from porcine Pcells. There is no statistically significant difference between SubSL and core sparks. N=50 SubSL and 50 core sparks, randomly chosen from 7 porcine hearts. Values were presented as mean +/- standard error.

C.2. Analysis of Propagating Spontaneous Ca^{2+}-transients ("Ca^{2+}-waves")

Two types of spontaneous, propagating Ca^{2+}-transients were observed. Small fluorescence transients ("Ca^{2+}-wavelet"; Fig. 23) were detected predominantly at the periphery of the Pcell SR. These wavelets propagated on short distances with high velocity (~1.6 mm/s) and exhibited amplitudes in the same range as Ca^{2+}-sparks.

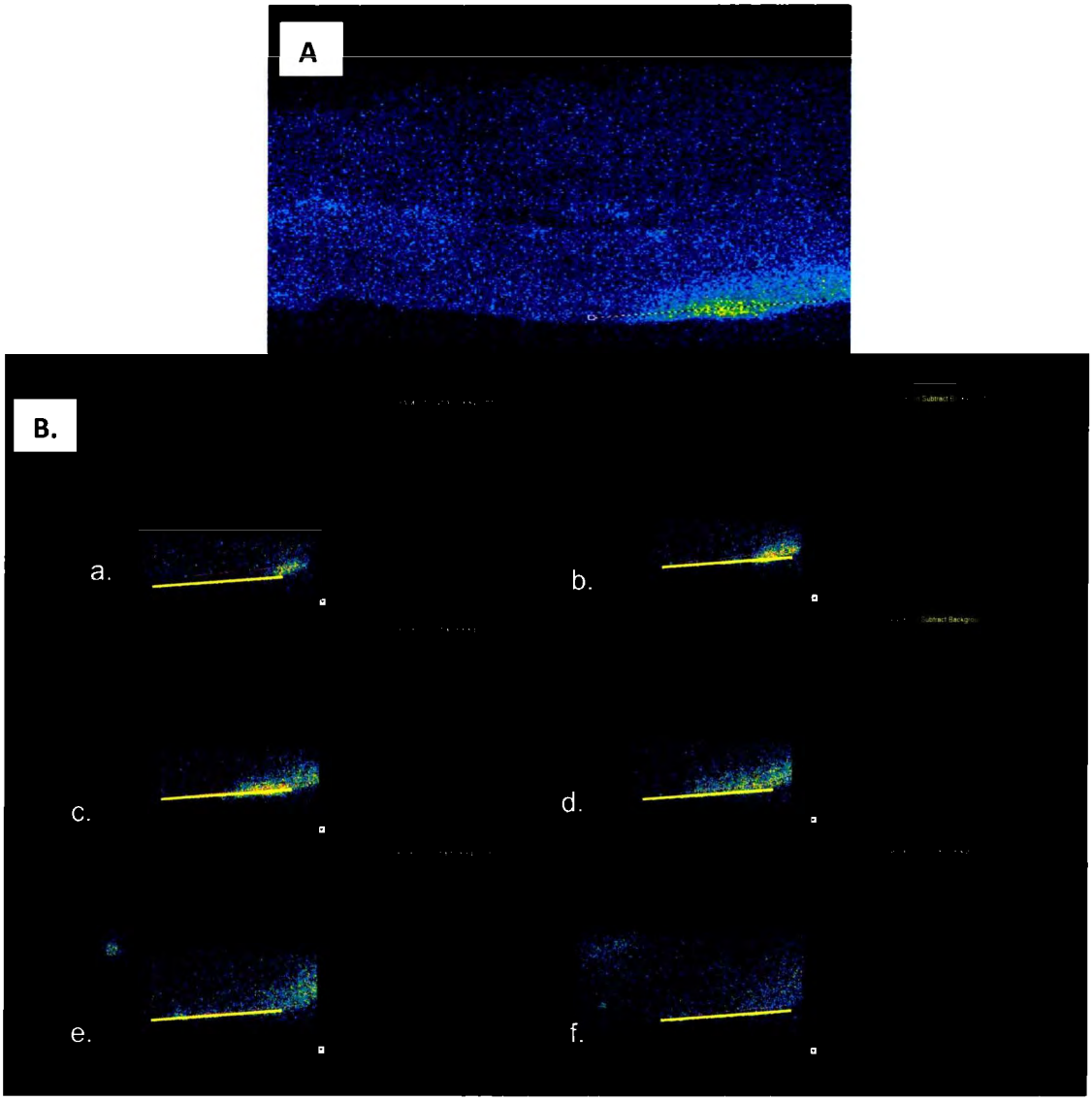

Figure 23: 2D confocal microscopy images showed the propagation of a Ca^{2+}-wavelets along the SubSL region of a porcine Pcell aggregate. Yellow trace lines showed fluorescence (pixels) vs. distance (µm). a) 2-cell aggregate of Pcells. The cell on the bottom was analyzed for functional Ca^{2+}-dynamics (B). B) a-f) Captured wavelet, with line scan application shown on cell and trace of Ca^{2+}-dynamics. Images were presented in pseudo color. *(Source: Jan 19 (4mM) 5)* Wavelets traveled at a velocity of approximately 1.6 mm/s.

Large waves were detected occasionally in the form of large, wide fluorescent transients extending over the full width of the cell and propagating longitudinally from cell to cell within the aggregates, so termed Cell Wide Waves (CWW, see Fig. 24).

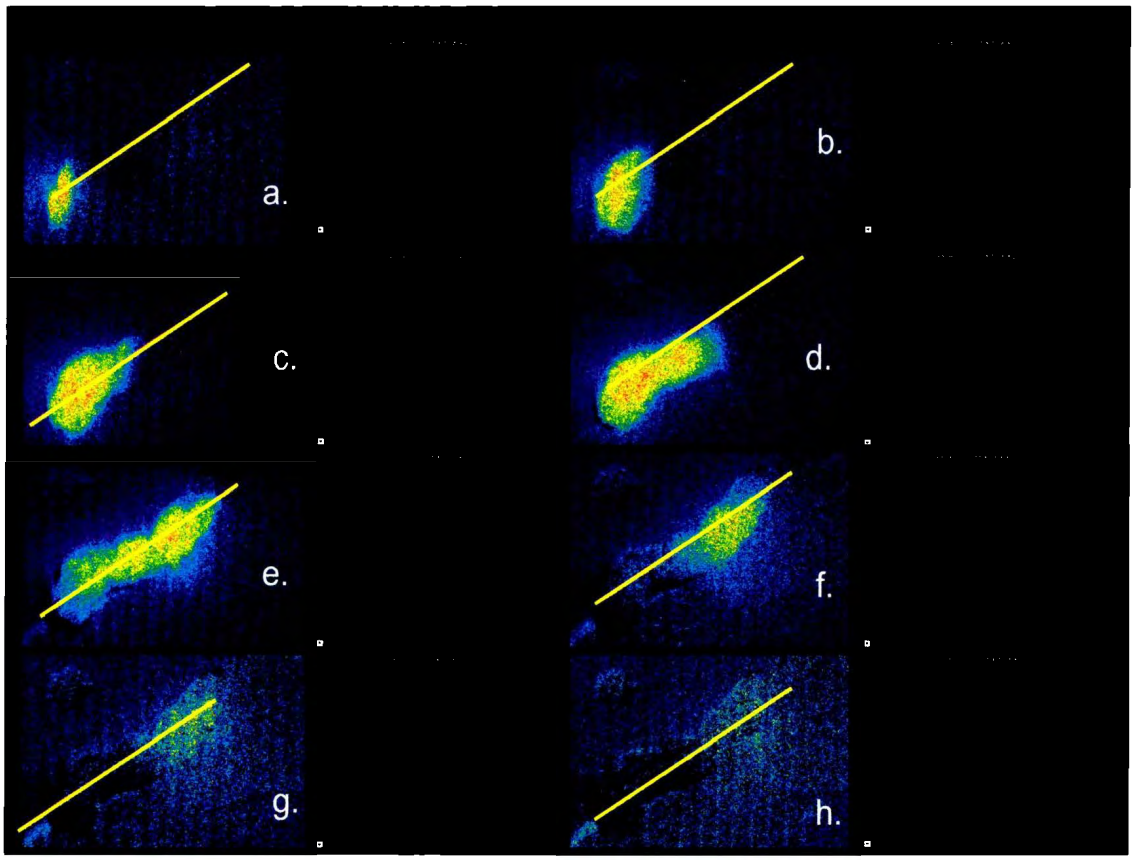

Figure 24: 2D confocal image of a Cell Wide Wave of Ca^{2+}, as it propagated though the Pcell core. Pcell pictured was part of an aggregate. Image presented in pseudo color. Trace lines showed fluorescence (pixels) vs. distance (µm). CWWs propagated at a velocity of approximately 1.5mm/s. *(Source: Dec 17 (4mM) 14)*

	Velocity (mm/s)	Amplitude (F/Fo)	Time to Rise (ms)	Time to Half Relaxation (ms)
Wavelets (n=11)	1.59±0.11	1.07±0.01	89.4±9.6	276±25
CWWs (n=8)	1.48±0.07 NS	1.15±0.06 NS	810.9±143 NS	1179±91 NS

Table 4: Comparison between small (wavelets) and large (CWWs) propagating Ca^{2+} transients in porcine Pcells (Ca^{2+}: 2mM; pH: 7.3, Temp: 25°C). N=11 wavelets and 8 CWWs, randomly chosen from 7 porcine hearts. Values presented as mean +/- standard error. NS: no statistical difference between wavelets and CCWs.

Comparison of the data collected characterizing the propagation velocity and time course of Ca^{2+} events (Table 4) indicated that there were no statistically significant differences between wavelets and CWWs ($P \geq 0.05$).

Therefore, unlike the immunofluorescence data presented in section A, our study of the spatiotemporal characteristics of Ca^{2+} events in section C did not support the existence of different RyR isoforms between the SubSL and the core of porcine Pcells and was not consistent with results obtained in canine Pcells *(Stuyvers et al. 2005).*

We were concerned that the discrepancies between immunofluorescence and characteristics of Ca^{2+} events were due the relatively small sample size of the study. Therefore, we elected to study the regional response of the Pcell to different SR-Ca^{2+} loads.

C.3. Analysis at External Ca^{2+}-Concentrations

The Ca^{2+}-sensitivity of the Ca-induced Ca-Release (or *CICR)* to SR-Ca^{2+} load was proposed to be different between RyR_2 and RyR_3 isoforms (*Stuyvers et al. 2005*). The Ca^{2+} sensitivity is set by the Ca^{2+} release threshold of the RyR, which in turn, is

determined by the intracellular Ca^{2+} level. Sobie and collaborators *(2006)* theorize that the relative insensitivity of the RyR to Ca^{2+} is a biological measure to ensure stability of the system. This RyR Ca^{2+} threshold is an important determinant of the frequency of Ca^{2+} events and of the propagation velocity of Ca^{2+} waves and, most importantly, differs between RyR_2 and RyR_3.

To detect a potential difference in the isoforms of RyR between SubSL and core regions in Pcells, we evaluated the Ca^{2+} sensitivity of the CICR in both regions by measuring the frequency of propagating Ca^{2+}-events (waves) and characteristics including the propagation velocity of waves (wavelets and CWWs) at various external Ca^{2+} concentrations ($[Ca^{2+}]_o$): 1,2,4 and 8 mM Ca^{2+}. Increasing external Ca^{2+}-concentration was anticipated to increase the Ca^{2+} load of the cell, which would bring the cell closer to the threshold of the initiation of CICR activity.

Fig. 25 showed that spark rate increased linearly with increasing $[Ca^{2+}]_o$ concentration up to 8 mM, in both SubSL and core regions. There was a statistically significant ($P<0.05$) difference between SubSL and core spark rate frequency at 4 mM Ca^{2+}, but, surprisingly, not at 8 mM although linear regression indicated even larger difference. This is likely to be due to the lower sample size (n=10) of Pcells examined at 8 mM Ca^{2+}.

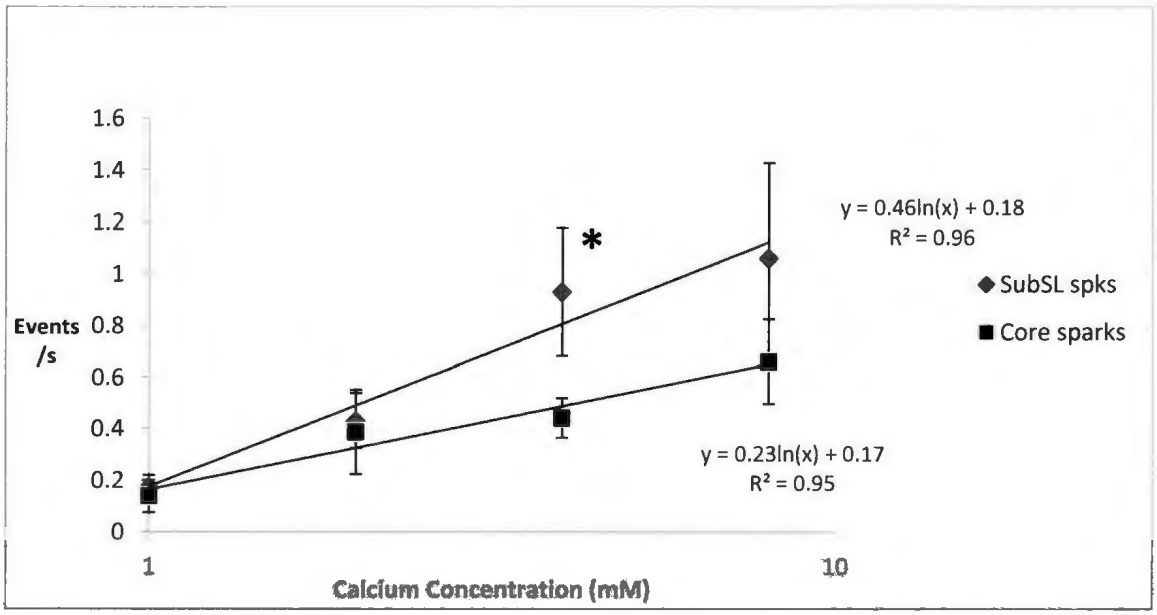

Figure 25: Event rate in the SubSL and core sparks vs. external Ca^{2+}- concentration. Data presented as mean +/- standard error. Both types of sparks increased in frequency with increasing Ca^{2+}- concentration following a linear relationship, but SubSL sparks increased at a greater rate. The difference between SubSL and core increases was statistically significant at 4mM Ca^{2+} (*P<0.05); as determined by ANOVA. SubSL spark event rate (sparks/s)=0.46ln([Ca^{2+}])+0.18 (R^2=0.96). Core spark event rate (sparks/s)=0.23ln([Ca^{2+}])+0.17 (R^2=0.95). Number of Pcells examined (N) = 20, 11, 20 and 10 at 1, 2, 4 and 8mM $[Ca^{2+}]_o$ respectively. These data were collected from 7 porcine hearts.

As shown in Fig. 26 below, counting the waves in the SubSL and core regions revealed an increase of Ca^{2+}-event rate with increasing extracellular Ca^{2+} concentration, up to 8 mM. Event rate increased linearly with Ca^{2+}-concentration. The increase in CWWs was significantly (P<0.05) lower than that of wavelets at 4 mM $[Ca^{2+}]_o$. As with the core and subSL sparks (Fig. 25), a change in frequency appeared at 8 mM Ca^{2+}, when linear regression was considered. The absence of significant difference in the ANOVA test, here again, is likely to be due to low sample size (n=10) of Pcells examined at this

concentration. Taking into consideration that wavelets were counted exclusively in the SubSL region, the results of Fig. 26 suggested that there was a larger Ca^{2+} sensitivity of CICR in the SubSL compared to the core.

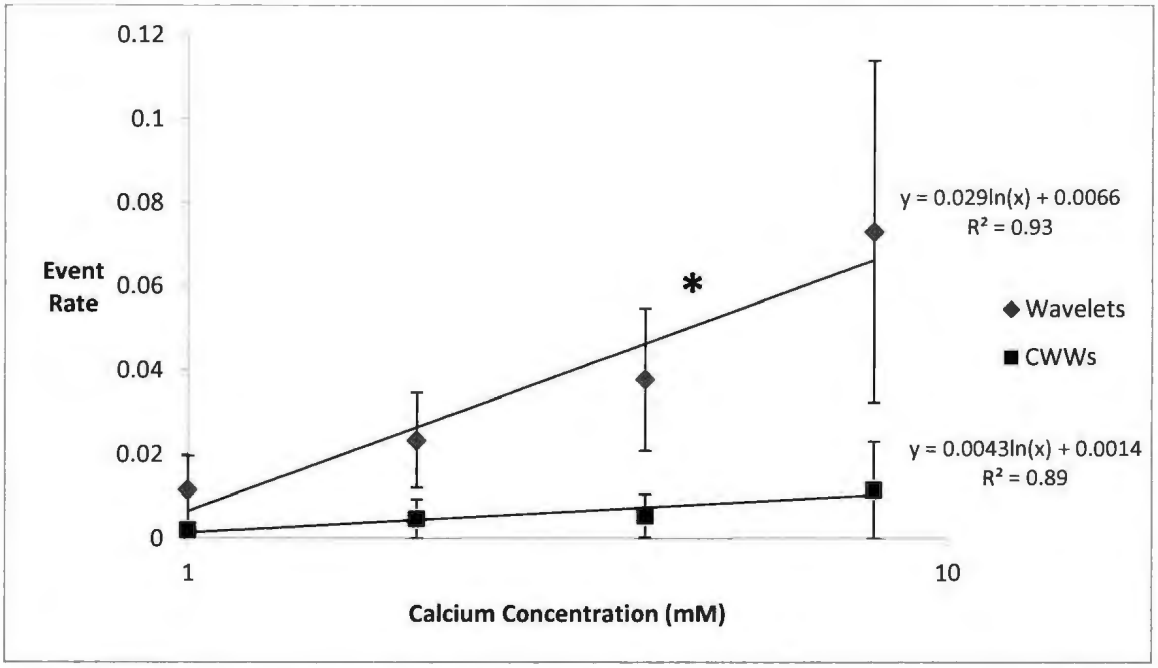

Figure 26: Event rate of wavelets and CWWs, with respect to varying external Ca^{2+}-concentration ($[Ca^{2+}]_o$) in porcine Pcells. Data presented as mean +/- standard error. A linear relationship was apparent with the increase in Ca^{2+}-transient frequency with increasing Ca^{2+}- concentration, but wavelets increased at a statistically significant ($P<0.05$), greater rate at 4 mM $[Ca^{2+}]$ as determined with ANOVA. Wavelet event rate=$0.029\ln([Ca^{2+}])+0.0066$ ($R^2=0.93$). CWW event rate=$0.0043\ln([Ca^{2+}])+0.0014$ ($R^2=0.89$). Number of Pcells examined (N) = 20, 11, 20 and 10 at 1, 2, 4 and 8mM $[Ca^{2+}]_o$ respectively. These data were collected from 7 porcine hearts.

Fig. 27 indicates a non-linear increase in the velocity of wavelets, with increasing external Ca^{2+}-concentration. This phenomenon is different than that observed for CWWs.

Therefore, the results of Fig. 27 suggest that wavelets and CWWs are created by different Ca^{2+}-wave generators. However, due to a relatively low number of samples, the increase of wavelet velocity and differences of wavelets versus CWWs were not confirmed statistically.

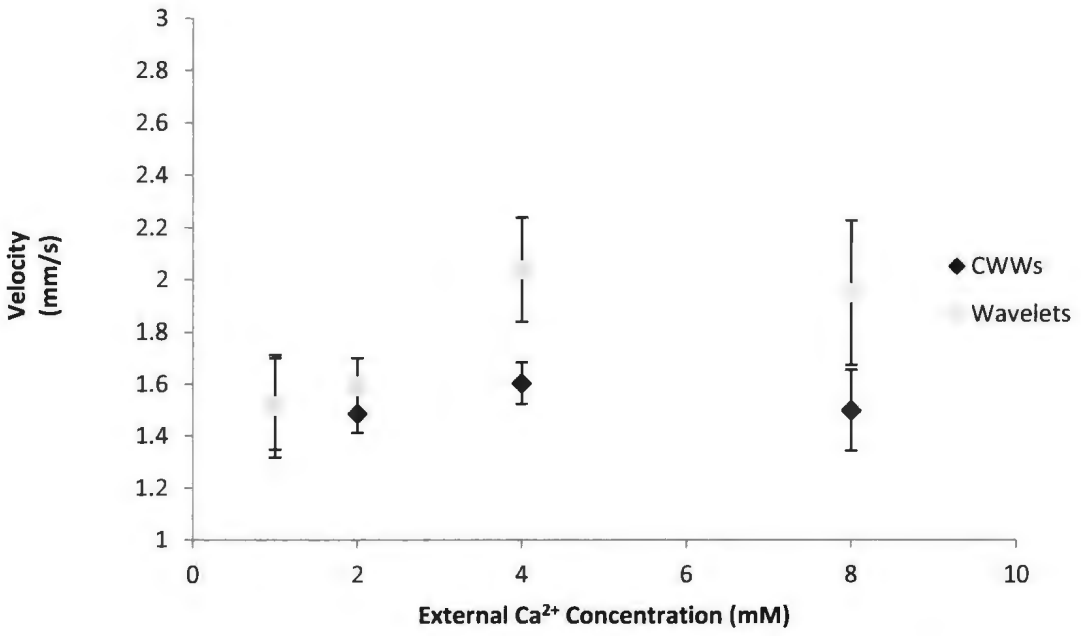

Figure 27: Comparison of velocity of wavelets and CWWs in porcine Pcells. There was no statistically significant difference between the velocity of wavelets (N=11 Pcells) and CWWs (N=8 Pcells). These data were collected from 7 porcine hearts.

The time course of wavelets and CWWs were measured at each Ca^{2+} concentration (1, 2, 4 and 8 mM). Amplitudes, rising times (T_{Rise}) and decay times ($T_{1/2Relaxation}$) are reported in Tables 5 and 6, respectively.

External $[Ca^{2+}]$ mM	Amplitude (F/Fo)	Time to Rise (ms)	Time to Half Relaxation (ms)
1 (n=6)	1.08±0.02	105.5±11.30	205±36
2 (n=4)	1.07±0.01	89.4±9.6	276±25
4 (n=11)	1.09±0.01	144.5±25	332±35
8 (n=3)	1.10±0.02	112±25	471±174

Table 5: Results from the qualitative analysis of wavelets in porcine Pcells: Amplitude, T_{Rise} and $T_{1/2Relaxation}$. Data presented as mean +/- standard error. No statistically significant differences (P>0.05) were found between the data groups. These data were collected from 7 porcine hearts. N=Number of Pcells examined.

External $[Ca^{2+}]$ mM	Amplitude (F/Fo)	Time to Rise (ms)	Time to Half Relaxation (ms)
1 (n=3)	1.20±0.04	213±80	612±94
2 (n=8)	1.15±0.06	811±143	1179±91
4 (n=5)	1.34±0.07	586±151	1175±258
8 (n=4)	1.29±0.09	1051±179	1149±35

Table 6: Results from the qualitative analysis of CWWS in porcine Pcells: Amplitude, T_{Rise} and $T_{1/2Relaxation}$. Data presented are mean +/- standard error. No statistically significant differences (P>0.05) were found between the data groups. These data were collected from 7 porcine hearts. N=Number of Pcells examined.

No differences were detected in the amplitude (F/Fo) and rising time of wavelets versus CWWs, when extracellular $[Ca^{2+}]$ was increased. Although not confirmed statistically, it was noted that the duration of decay ($T_{1/2Relaxation}$) showed an increase with

$[Ca^{2+}]_o$ and the duration of the decay of the wavelets increased linearly with increasing $[Ca^{2+}]_o$ (Fig. 28).

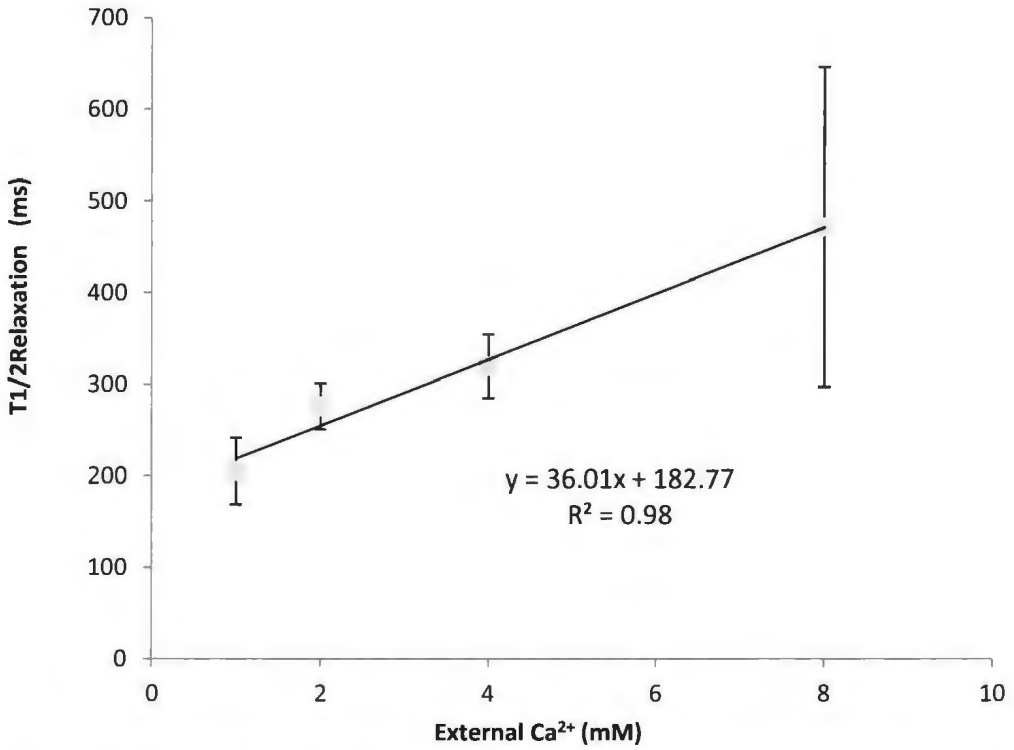

Figure 28: Time to Half Relaxation of wavelets (ms) in the porcine Pcell model. $T_{1/2Relaxation}=36.01[Ca^{2+}] + 182.77$. $R^2=0.98$. Number of Pcells examined (N) = 6, 11, 11 and 3 Pcells at 1, 2, 4 and 8 mM extracellular Ca^{2+} respectively. There was no weighting of any values. These data were collected from 7 porcine hearts.

D. Pharmacological characterization of the model of Centripetal Ca^{2+} activation in porcine Pcells

A single RyR isoform (RyR_2) modulated SR Ca^{2+} release and CICR in ventricular myocytes. In canine Pcells, the same phenomena were governed by 3 different forms of SR-Ca^{2+} channels: 1) the classical "cardiac" RyR_2, 2) the "neuronal" RyR isoform, RyR_3 and 3) the IP_3R_1 Ca^{2+} channel, which was activated by phosphatidyl inositol. RyR_3 and IP_3R_1 were therefore specific to the Ca^{2+} handling system of Pcells and were fundamental

components of the Centripetal Ca^{2+} -Activation System (see *Background* section for further elaboration).

To determine whether porcine Pcells utilized the same system of Ca^{2+}-activation, specific pharmacological modulators were used to assess the involvement of RyR_3 and IP_3R_1.

The muscle relaxant dantrolene was used as a specific inhibitor of RyR_3-Ca^{2+} release. IP_3R Ca^{2+} -release was tested in response to specific inhibitors Xestospongin-C and 2APB and the effects of IP_3/BM, an activator of intracellular IP_3 production was evaluated.

D.1. Modulation of RyR_3 Ca^{2+} release

Fig. 29A showed that exposure of Pcells to 1 μM dantrolene decreased the spark rate in both the SubSL (Fig. 29A.a) and the core (Fig. 29A.c). However, the kinetics of this decrease differed between the SubSL and the core. The dantrolene-induced inhibition of SubSL sparks occurred immediately upon applications of the drug, whereas the effect on the core sparks occurred after longer (≥1min) exposure to the drug. In the same experiments, a reduction in the frequency of wavelets was observed in presence of dantrolene, suggesting that this drug affected the SubSL region of the SR more than the core (Fig. 29.A.b).

In some experiments, 10 μM of ryanodine, a non-isoform selective inhibitor of RyR (Báez-Ruiz and Diaz-Mu□oz, 2011), was added during the effect of dantrolene. As shown by the representative examples of Fig. 29B, the addition of ryanodine further

reduced the spark activity remaining after 15 min of dantrolene exposure. As ryanodine inhibits all isoforms of RyR, it was not surprising to find that SubSL and core sparks were both inhibited.

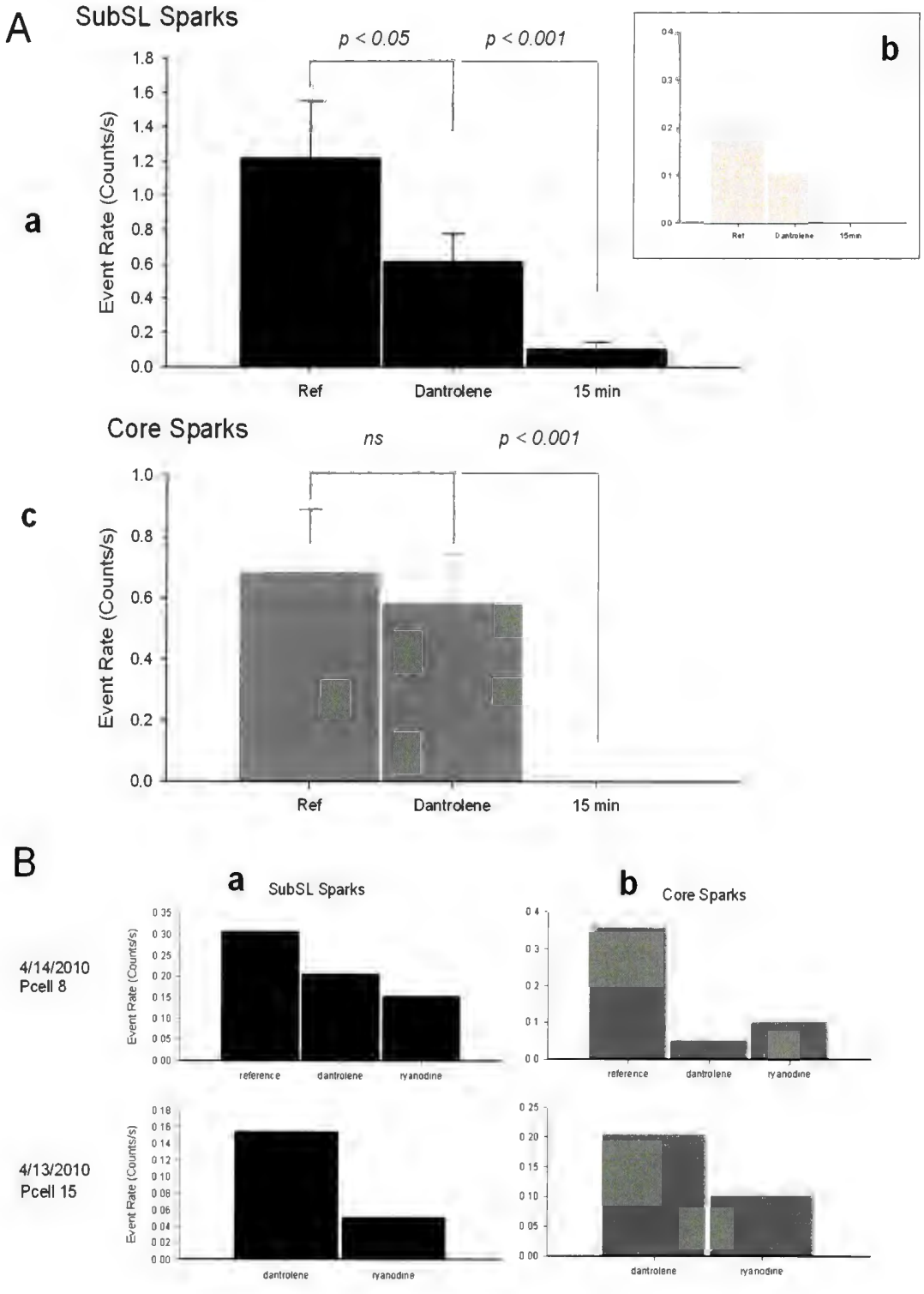
A
SubSL Sparks
p < 0.05
p < 0.001
a
b
Event Rate (Counts/s)
Ref
Dantrolene
15 min
Core Sparks
ns
p < 0.001
c
Event Rate (Counts/s)
Ref
Dantrolene
15 min
B
a
SubSL Sparks
b
Core Sparks
4/14/2010
Pcell 8
Event Rate (Counts/s)
reference
dantrolene
ryanodine
4/13/2010
Pcell 15
Event Rate (Counts/s)
dantrolene
ryanodine

Figure 29: The effect of dantrolene on Ca^{2+} release events in the SubSL and the core of porcine Pcells. The spark frequencies (counts/second) were determined in the SubSL (Panel A.a) and the core (Panel A.c) of 13 Pcells in the presence of 1 μM dantrolene ($[Ca^{2+}]$=2mM; 25°C; pH 7.4). These data were collected from 5 porcine hearts. There was a statistically significant difference between the event rate of sparks in the SubSL immediately after the administration of dantrolene ($P<0.05$), as well as after 15 minutes ($P<0.001$); as determined with ANOVA. Wavelets were counted under the same conditions (Panel A.b). In some representative cells, 10 μM ryanodine was used, as shown in the two examples of Panel B. Note that additions of ryanodine further decreased the spark rate in both the SubSL and core regions. As these are representative examples to show the effects of ryanodine on porcine Pcells, no statistical analysis was performed on these cells.

D.2. Modulation of IP_3R_1 Ca^{2+}-Release

The involvement of IP_3R_1 within the Ca^{2+} handling system of porcine Pcells was tested using 2 specific inhibitors: 2APB and Xestospongin-C.

Addition of 2APB caused a statistically significant reduction in the frequency of Ca^{2+}-sparks in the NearSL region at 4 mM extracellular $[Ca^{2+}]$ during short (1-5 minutes) and long (>5 minutes) term exposure to the agent. No other significant changes in the core sparks, wavelets nor CWWs were observed on application of 2APB (Fig. 30).

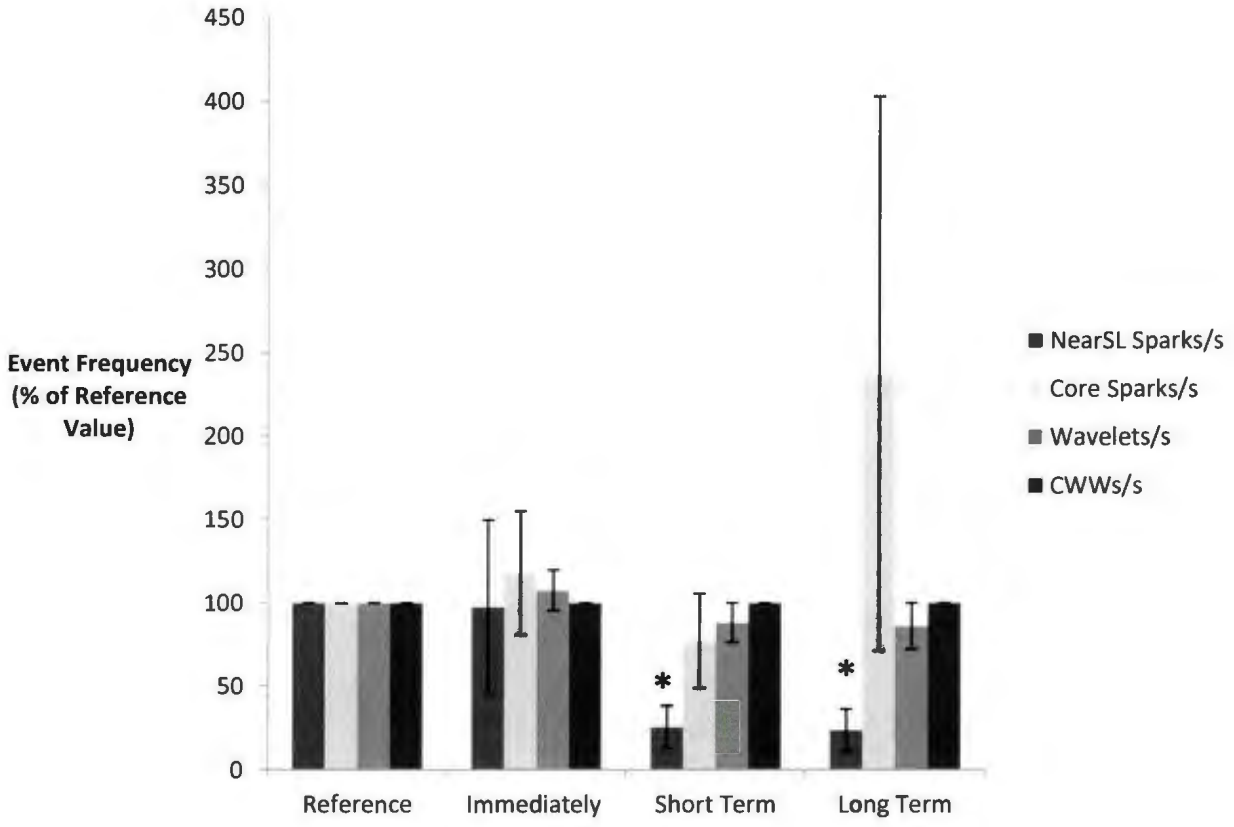

Fig. 30: Effects of 2APB on Ca^{2+}-event frequency in Pcell aggregates. All data points are presented with respect to a reference event rate. Note the reduction of the spark rate in the NearSL (*$P < 0.001$). There are no significant reductions in the frequency of core sparks, wavelets and CWWs upon addition of 2APB. N=10Pcells, from 3 porcine hearts. Data were analyzed statistically using ANOVA and unpaired Student's T-tests with all data points being compared to the reference value. Average reference values for NearSL sparks, core sparks, wavelets and CWWs were 1.68, 0.73, 0.65 and 0, respectively.($[Ca^{2+}]$=4mM, 25°C, pH 7.4) Here 'Reference' is a cell which has not been modulated with any pharmacological agents. The number of Ca^{2+}-transients observed in this cell was considered (100% of) the Reference Value. All other values shown in this chart are percentages of the Reference (un-modulated by 2APB) value. 'Immediately' is the frequency of Ca^{2+}-activity in a cell immediately after the agent is added, 'short' term is the frequency between 1 and 5 minutes following administration of 2APB. 'Long term' is the frequency >5 minutes.

Addition of 3 μM 2APB induced a statistically significant reduction of the NearSL spark rate in the short and long term. Meanwhile, 2APB simultaneously showed an increase in Ca^{2+}-spark rate within the core. The details of the variations of spark rate in the NearSL and in the core are given in Fig. 31. Under the same conditions ($[Ca^{2+}]$ = 4mM, 25°C, pH 7.4), 2APB had no statistically significant effect on the frequency of wavelets and CCWs (Fig. 30). Furthermore, addition of 2APB was shown to cause a significant decrease in the amplitude (F/Fo) of NearSL sparks, but no significant difference in core sparks (Fig. 32).

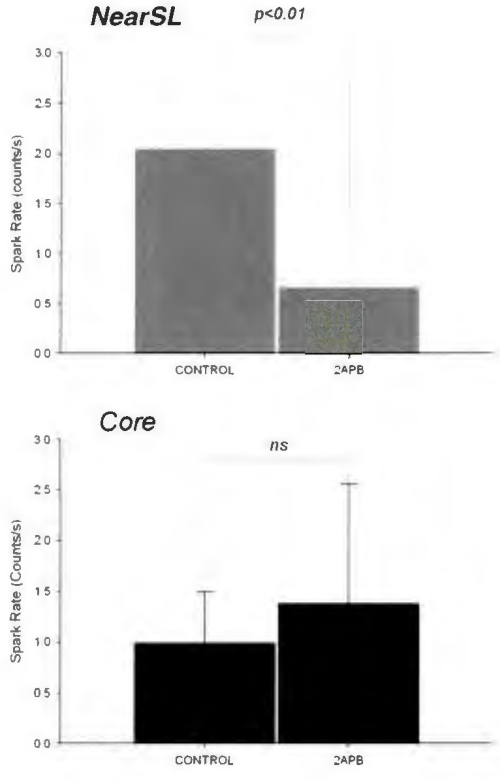

Figure 31: Effect of 2APB on spark rate in the NearSL and core of Pcells (Ca^{2+} 4mM; pH 7.4, Temp 25°C). N=5 Pcells, from 5 porcine hearts. There was a significant difference (P<0.01) in the NearSL spark rate following administration of 2APB, as determined by an unpaired Student's T-test. 'Control' group is porcine Pcells in physiological conditions, without 2APB. Data are presented as the mean of the spark rate (counts/second) +/- standard error.

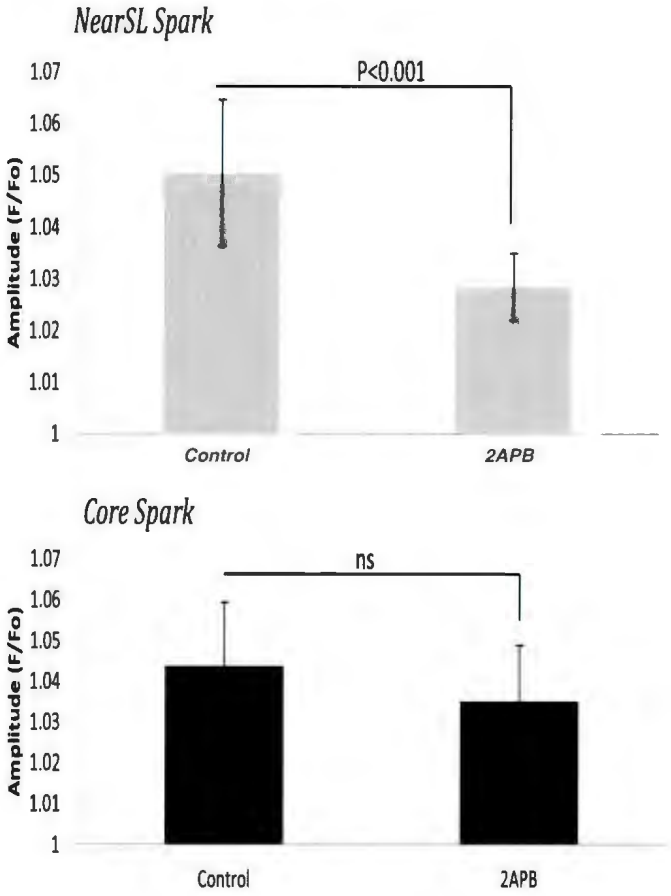

Figure 32: 2APB effect on spark amplitude (F/Fo) in the core and NearSL of Pcells (Ca^{2+} 4mM; pH 7.4, Temp 25°C); N=5 Pcells from 5 porcine hearts. There was a statistically significant difference (P<0.001) between the Control (physiological conditions, no 2APB) NearSL spark amplitude and that following 2APB administration, as determined by a Student's T-test. Data are presented as mean +/- standard error.

As shown in Fig. 33, exposure to 10-100 μM of Xestospongin-C, another specific inhibitor of IP_3R_1, reduced the frequency (counts/s) of NearSL sparks (N= 5; P<0.003).

Meanwhile, Xestospongin-C did not affect the incidence of core sparks, wavelets or CWWs (Fig. 33).

There was no statistically significant difference observed at 4 mM $[Ca^{2+}]_o$ in the amplitude (F/Fo) of the NearSL and core sparks after the administration of Xestospongin-C.

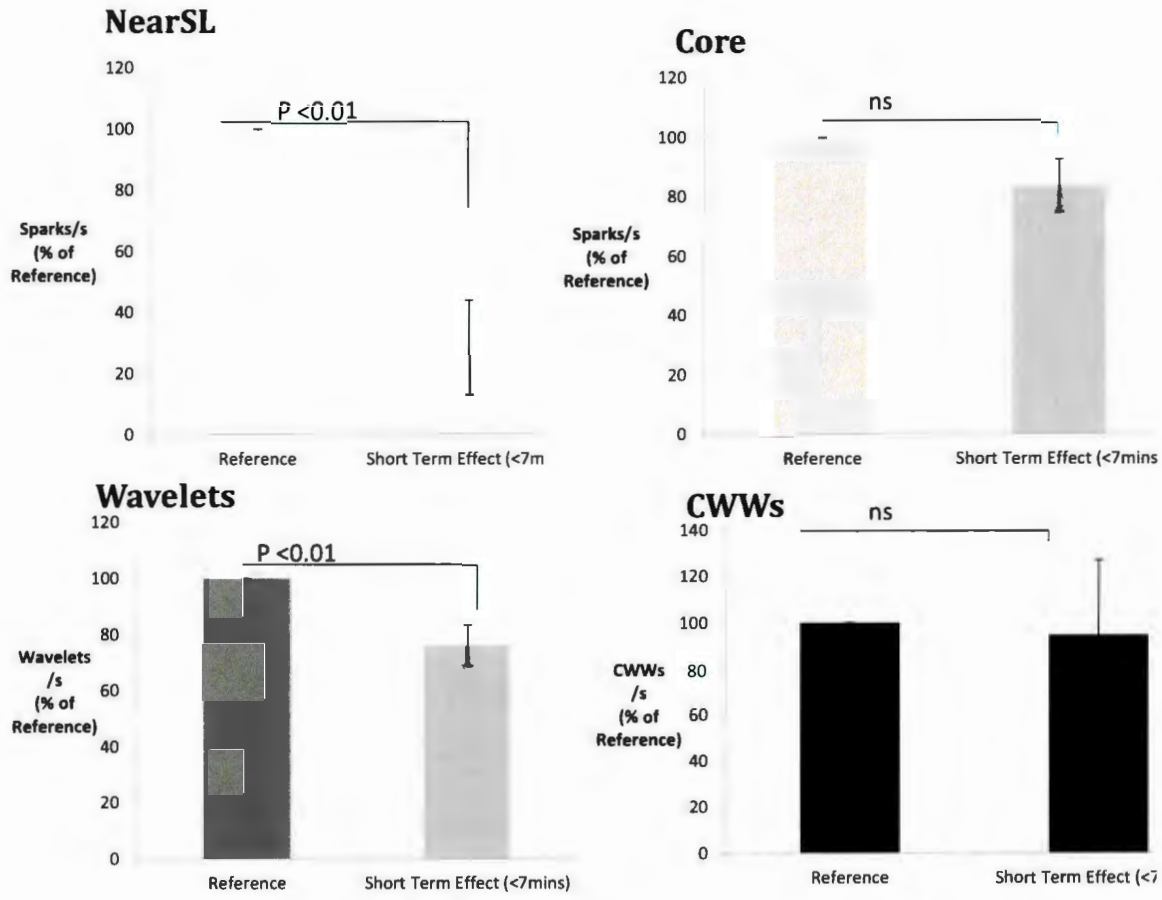

Fig. 33: Effects of Xestospongin-C on the frequency of Ca^{2+}-events/s in Pcell aggregates at 4 mM $[Ca^{2+}]_o$ (pH 7.4, Temp 25°C). The difference compared to the Reference Pcell (un-modulated by Xestospongin-C) was significant when P<0.001, as determined by a Student's T-test. (NS: no statistically significant difference). Values are expressed as % of Reference Value. Standard Error bars are expressed. N=7 Pcells from 3 porcine hearts.

Attempts were made to stimulate the metabolic pathway of IP_3 production and, thus, activate IP_3R_1 near the plasma membrane by using the liposoluble agent IP_3/BM. The effects of IP_3/BM in the presence of 2 mM and 4 mM Ca^{2+} are shown in Fig. 34 and 35, respectively. As these were preliminary investigations, trends are included as individual cell dynamics, and no statistical tests were performed.

In the representative examples below, a large increase of spark rate was observed in the NearSL region immediately after the addition of IP_3/BM (upper panels in Fig. 34, 35). The spark rate was restored immediately when IP_3/BM was removed, and the preparation was washed with the test solution (see arrow in upper panel Fig. 34). During continuous exposure to IP_3/BM, the same increase in spark rate was followed by a more progressive return to control (upper panel in Fig. 35). Under the same conditions, similar but less pronounced variations of spark rates were also observed in the core (lower panels in Fig. 35 and 36). A comparison of the effect of IP_3/BM on spark rate between the core and SubSL regions is illustrated in middle panel of Fig. 35.

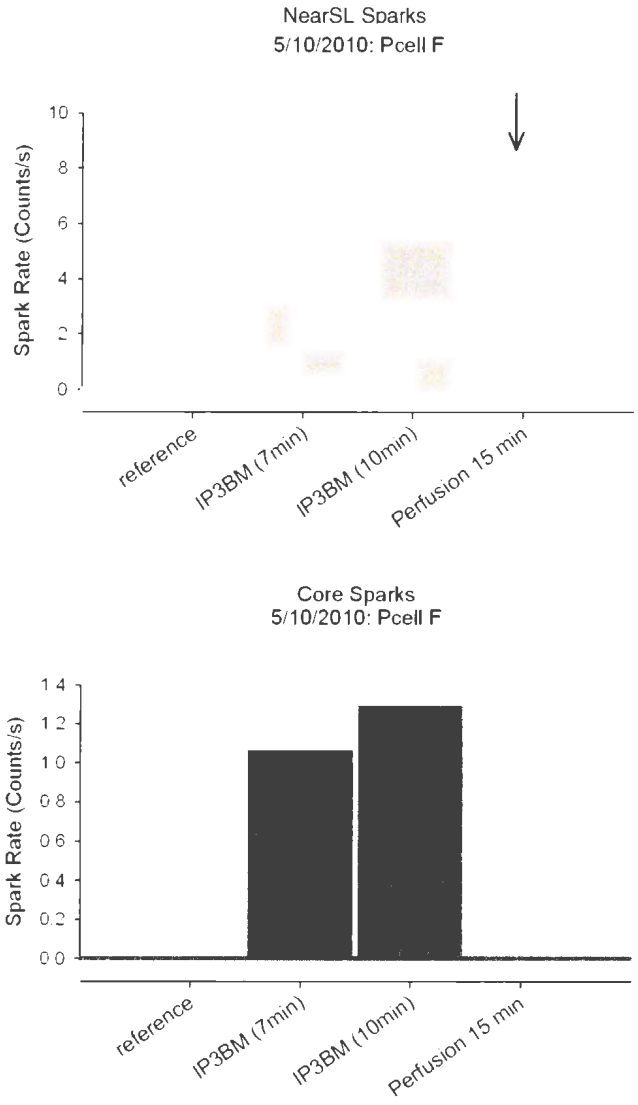

Fig. 34: Representative example of IP_3/BM effect on spark rate (counts/s) in the core and NearSL region of one porcine Pcell aggregate at 2mM $[Ca^{2+}]_o$, 25°C, pH 7.4. Preliminary data: N=1. *(Source: May 10PcellK)*

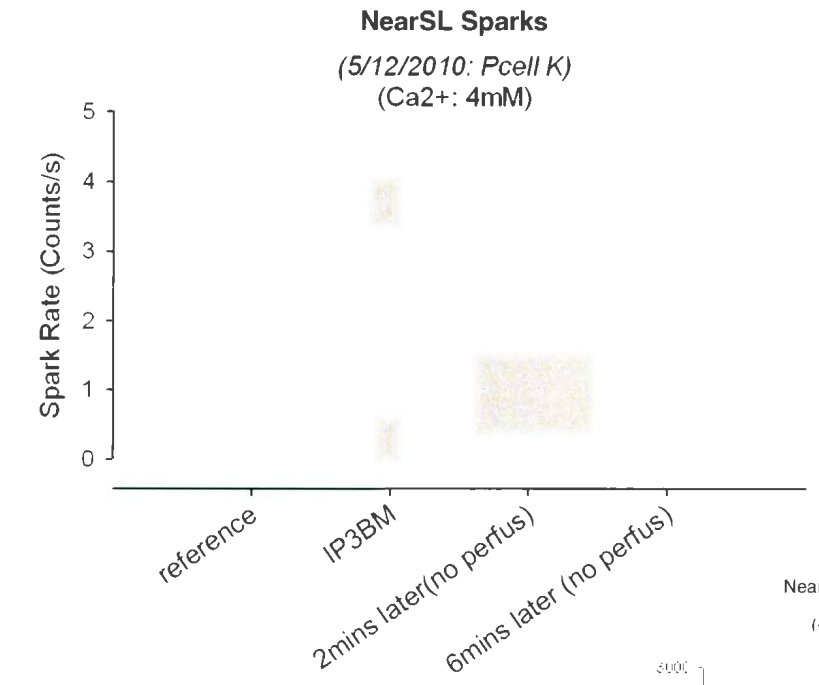
NearSL Sparks
(5/12/2010: Pcell K)
(Ca2+: 4mM)
Spark Rate (Counts/s)
0
1
2
3
4
5
reference
IP3BM
2mins later(no perfus)
6mins later (no perfus)

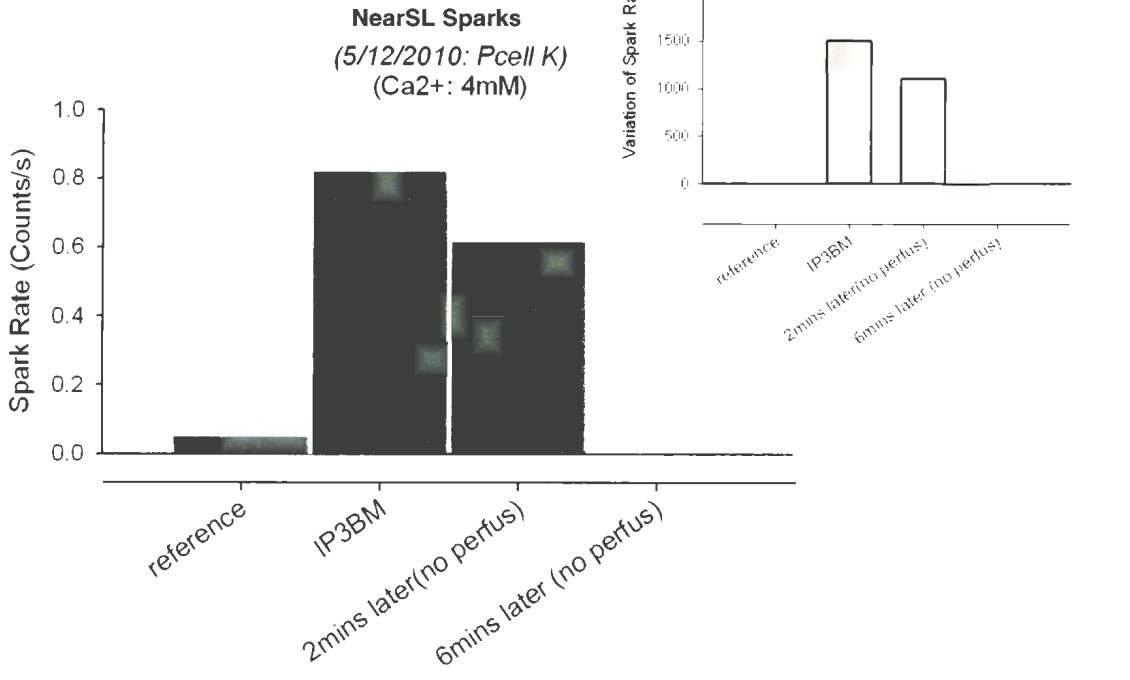
NearSL Sparks
(5/12/2010: Pcell K)
(Ca2+: 4mM)
Spark Rate (Counts/s)
0.0
0.2
0.4
0.6
0.8
1.0
reference
IP3BM
2mins later(no perfus)
6mins later (no perfus)
NearSL vs. Core Sparks
(5/12/2010: Pcell K)
(Ca2+: 4mM)
Variation of Spark Rate (%Ref)
%NearSL Sparks
%Core Sparks

Fig. 35: Representative example of the effect of IP_3/BM on spark rate (counts/s) in the core and NearSL region of one porcine Pcell aggregate at 4 mM $[Ca^{2+}]_o$. Preliminary: N=1. *(Source: May10PcellF)*

E: Summary

Specific pharmacological inhibitors of known Ca^{2+}-generators yielded changes in the intracellular Ca^{2+}-dynamics of porcine Pcells. Dantrolene, an inhibitor of RyR_3, caused an immediate and significant decrease in the frequency of SubSL sparks (Fig.29), with no immediate effect on other cellular regions. 2APB, a specific inhibitor of IP_3R-Ca^{2+} release significantly reduced the frequency and amplitude of sparks in the NearSL (Fig. 30, 31 and 32). Similarly, Xestospongin-C, another inhibitor of IP_3R, significantly reduced the spark frequency in the NearSL (Fig. 33), with no effect on the cell core. It was interesting to notice the trend that the remaining small spark activity was decreased by the ryanodine (Fig. 29) a non- isoform specific inhibitor of RyR. However, this finding was tested in only a few samples, so no statistical significance was identified.

Specific immunostaining showed that RyR was found throughout the cell SR (Fig. 14). The SR membrane expressed RyR_2 (Fig.18), RyR_3 (Fig. 15 and 16) and IP_3R_1 (Fig. 17) in the cell core, SubSL and NearSL, respectively.

Discussion & Interpretation

Working Hypothesis: in the porcine cardiac Purkinje fiber, there are 3 layers of Ca^{2+}-generators which link excitation of the plasma membrane with SR Ca^{2+} release in the core.

"Centripetal" Activation occurs through the sequential excitation of three distinct regions of the SR in the porcine Pcell: 1) the 'NearSL region' filled with IP_3R_1; 2) the 'SubSL region' filled with RyR_3; 3) and the 'core region,' filled with RyR_2.

For convenience, in our discussion, this working hypothesis was subdivided into 3 "subhypotheses" that were addressed separately.

Subhypothesis 1: There is a *NearSL region*, containing IP_3R_1, at the periphery of the SR, in close apposition with the sarcolemma. This layer contributed to the triple layered system of Ca^{2+}-generators in Pcells, as described in the canine model (*Stuyvers et al., 2005*).

In our study, the NearSL region of the porcine Pcell was examined using immunofluorescence specific for IP_3R_1 (Fig. 17), RyR (Fig. 14) and RyR_2 (Fig. 18). Alpha-actinin immunofluorescence (Fig. 10) and electron microscopy studies (Fig. 12 and 13) indicated that Pcells, like myocytes, were filled with abundant myofibrils. IP_3R_1 was found in the NearSL region; in a thin layer approximately 1.7-2μm thick. RyR_2 was found in all regions of the Pcell SR (Fig. 18) including the NearSL region.

In porcine Pcells, our data supported the existence of thin region of SR adjacent to the sarcolemma, wherein Ca^{2+}-specific proteins IP_3R_1 and RyR_2 co-exist. These findings were consistent with previous results from canine Pcells (*Stuyvers et al., 2005*).

Our study of the Ca^{2+}-dynamics between 1 and 8 mM external [Ca^{2+}] (Fig. 25) revealed a major difference in spark activity between the core and the periphery of the cell. The sparks occurred at a higher rate in the periphery than in the core at 4 mM Ca^{2+} (Fig 25). As well, the spark rate vs. $[Ca^{2+}]_o$ relationships showed that peripheral sparks were more sensitive to external [Ca^{2+}] than core sparks (Fig. 25), which supported the idea that Ca^{2+} channels responsible for sparks were different between the periphery and the core regions. The histograms in Fig. 22a and 22d display the wide range of spark amplitudes in the SubSL. As suggested previously (*Hirose et al. 2008*), these large Ca^{2+}-sparks with large amplitudes and T_{Rise} were primarily due to the activation of IP_3R_1, while smaller sparks were caused by the Ca^{2+} release from RyR_2.

The reduction in the spark frequency in the NearSL region by inhibition of IP_3R_1 (Xestospongin-C (Fig. 33) and 2APB (Fig. 30, 31 and 32)) confirmed the presence of abundant IP_3R_1 in this region. The same reduction of spark frequency in presence of 2APB in the NearSL region was observed previously in canine Pcells (*Hirose et al., 2008*). IP_3/BM , which activates the production of IP_3, was used to activate IP_3R_1. We found an increase of NearSL spark frequency in the representative (n=1) Pcell aggregates examined (Fig. 34, 35).

The addition of 2APB caused a significant decrease of NearSL spark count (sparks/s), while it caused a slight (although not significant) increase in the core sparks (Fig. 31). These observations are consistent with the existence of a single SR compartment with membranes containing different gates. Blockade of one type of gate (the IP_3R in the NearSL), causes a transitory increase of spark activity at the other active gates (the RyR_2 in the core). Then the spark activity slows down as the SR-Ca^{2+} content becomes depleted.

Subhypothesis 2: There is a *SubSL region* of the SR, located between the NearSL region and the cell core. The results from immunofluorescence (Fig. 15, 16) supported the existence of RyR_3 within a 4-6μm region in the SR, just inside of the sarcolemma. In addition, immunofluorescence showed an apparent 2μm void of RyR_2 (Fig. 18) in the SR, just inside of the sarcolemma. We found that immuno-staining for RyR_3 was overlying this void (Fig 15, 16).

Study of Ca^{2+}-dynamics at varying external Ca^{2+}-concentrations (Fig. 25, 26) revealed specific small Ca^{2+}-waves ("wavelets") in the region corresponding to RyR_3 location. At all extracellular Ca^{2+}-concentrations examined (1, 2, 4 and 8 mM Ca^{2+}); the frequency of wavelets was higher than that of CWWS (Fig. 26). This suggested that the SR Ca^{2+}-channels which were creating wavelets could be activated more readily than those which were creating CWWs. Murayama (*1999*) reported that the threshold of activation for the RyR_3 is between 0.1and 1μM cytosolic Ca^{2+}, which was significantly lower than that reported by Kong and collaborators *(2008)* for RyR_2 , which was 3mM

cytosolic Ca^{2+}. Both of these experiments were performed at 25°C, as is the data presented here, removing Q10 as not a factor for error. We propose therefore, that in porcine Pcells, wavelets occur as a result of the activation of RyR_3s, while CWWs are due to the activation of RyR_2s.

The core and SubSL sparks were inhibited by ryanodine (Fig. 29Ba and Fig. 29Bb) although not significant because of a low sample size. This confirmed that these SubSL and core sparks were generated by RyRs, but did not provide any information regarding isoform specificity of the sparks. Fig 29Aa and Fig29Ab showed that on the addition of dantrolene, there was an immediate decrease in SubSL sparks. This suggested that SubSL sparks resulted from RyR_3 Ca^{2+}-channels. Fig 29Ac showed that there was not this initial decrease in core sparks when dantrolene was added, suggesting a difference in the nature of SR Ca^{2+} channels between SubSL and core regions. Because Ca^{2+}-activity was selectively inhibited by dantrolene, the channel in the SubSL was likely RyR_3. However, the channels in the core were not immediately inhibited by dantrolene but were fully blocked by ryanodine, suggesting the presence of another RyR isoform in the cell core.

Subhypothesis 3: The third region of SR Ca^{2+}-generators in the porcine Pcell is observed uniformly throughout the core of the cell.

Immunofluorescence showed the presence of RyR_2 throughout the core SR of the Pcells (Fig 18). The RyR_2 antibodies were arranged in striations, matching those of the sarcomeric z-discs, as shown by the immunofluorescence of α-actinin (Fig. 9 and 10).

Analysis of Ca^{2+}-dynamics at varying extracellular Ca^{2+}-concentrations (Fig. 25) showed abundant regular Ca^{2+}-sparks in the core region, while large propagating CWWs occasionally appeared propagating along the cell-aggregates (Fig 26). These events have been studied using pharmacological modulators specific for receptors in the NearSL and SubSL regions. The frequency of these events were decreased with the addition of ryanodine (Fig. 29Ba and 31Bb), implying that core sparks were the result of one or more isoforms of RyR. Agents which affected the spark frequency in the NearSL or SubSL by immediately modulating the IP_3R_1 or RyR_3 (respectively) caused no statistically significant changes in the core spark frequency (Fig. 29-33).

Potential Pitfalls: First, the success rate of IP_3R_1 staining with specific antibodies was generally poor. One possible explanation is inappropriate dilutions of the antibody, as the suppliers did not always have recommended dilution factors. Although immunostaining was not always consistent, it was still occasionally successful and yielded similar results with previous data of the literature, thus supporting the specificity of the antibody. An alternative explanation is that the permeabilization of the cells by the detergent TX100 may have affected the integrity of the targeted proteins under the sarcolemma in some

cells and could alter the reactivity of the specific antibodies. Finally, the elliptic cross-section of the cells and the flattening of the cells under the coverslip may have made the specific observation of the core region difficult by confocal microscopy. In these flattened cells, the probability that the focus was set close to the top or the bottom of the cell was high and number of observations may have actually reported sections mostly across NearSL region. Particularly, this may have given the impression of a uniform non-specific staining of IP_3R_1 throughout the cell, which was seen frequently in the data set.

Conclusion

The results of this thesis support the idea of a unique mechanism of spontaneous Ca^{2+} activation in the cardiac Purkinje cells of large mammalian hearts: which is a triple layered system. This is different than the conventional model of excitation contraction coupling, seen in ventricular myocytes. The triple layered system consists of RyR_2, RyR_3 and IP_3R in the core, SubSL and NearSL respectively.

The objective of this project was to confirm in a large mammalian species, such as swine, that the cellular physiology of Purkinje fibers is governed by a unique and complex mechanism of Ca^{2+} handling. The fact that Ca^{2+} is an important factor of the electrical activity of Purkinje tissue implicates that any Ca^{2+} abnormality in Pcells is likely to cause cardiac rhythm disorders such as life threatening ventricular tachycardias. Our results can be used in further studies of pro-arrhythmic Ca^{2+} activity in Purkinje tissue after myocardial infarction, which may originate in one of the elements of the triple layered system of Ca^{2+} generators. The evidence that similar complex system exists in

porcine heart as well is important because, associated with previous observations of canine Purkinje, it suggests that human cardiac conduction system obey the same model, thereby raising the perspective of controlling the source of lethal post-MI arrhythmias.

References

Advanced Imaging Concepts Inc. Principles of the Microlens-enhanced Nipkow Disc Scanning Technology. 2010 [Accessed July 3, 2010. Available from: http://www.aic-imagecentral.com/products/pdfs/Principles_spinCSU.pdf]

Armstrong MR, Boyden K, Browning ND, Campbell GH, Colvin JD, DeHope WJ, Frank AM, Gibson DJ, Kim JS, King WE, LaGrange TB, Pyke BJ, Reed BW, Shuttlesworth RM, Stuart BC, Torralva BR. Practical considerations for high spatial and temporal resolution dynamic transmission electron microscopy. Ultramicroscopy. 2007; 107(4-5):356-67

Arnar DO, Bullinga JR, Martins JB. Role of the Purkinje system in spontaneous ventricular tachycardia during acute ischemia in a canine model. Circulation. 1997; 96(7):2421-9

Báez-Ruiz A, Diaz-Mu□oz M. Chronic inhibition of endoplasmic reticulum calcium-release channels and calcium-ATPase lengthens the period of hepatic clock gene Per1. Journal of Cardiac Rhythms. 2011; 9:6.

Bigger JT, Fleiss JL, Kleiger R, Miller JP, Rolnitzky LM. The relationships among ventricular arrhythmias, left ventricular dysfunction, and mortality in the 2 years after myocardial infarction. Circulation. 1984; 69(2): 250-258.

Bode K, Hindricks G, Piorkowski C, Sommer P, Janousek J, Dagres N, Arya A. Ablation of polymorphic ventricular tachycardias in patients with structural heart disease. Pacing and Clinical Electrophysiology (PACE). 2008; 31(12):1585-91

Boyden PA, Albala A, Dresdner KP Jr. Electrophysiology and ultrastructure of canine subendocardial Purkinje cells isolated from control and 24-hour infracted hearts. Circulation Research. 1989; 65:955-970

Boyden PA, Barbhaiya C, Lee T, ter Keurs HEDJ. Nonuniform Ca^{2+}-transients in arrhythmogenic Purkinje cells that survive in the infarcted canine heart. Cardiovascular Research. 2003; 57: 681-693

Boyden PA, Chirag B, Taehoon L, ter Keurs HEDJ. Nonuniform Ca^{2+} transients in arrhythmogenic Purkinje cells that survive in the infarcted canine heart. Cardiovascular Research. 2003; 57: 681-693

Boyden PA, Pinto JM. Reduced calcium currents in subendocardial Purkinje myocytes that survive in the 24- and 48- hour infarcted heart. Circulation. 1994; 89(6): 2747-59

Boyden PA, Pu J, Pinto J, ter Keurs HEDJ. Ca^{2+} transients and Ca^{2+} waves in Purkinje cells, role in action potential. Circulation Research. 2000; 86(4): 448-55

Brette F, Salle L, Orchard CH. Quantification of calcium entry at the T-tubules and surface membrane in rat ventricular myocytes. Biophysical Journal. 2006; 90(1):381-389

Bridge JHB, Ershler PR, Cannell MB. Properties of Ca^{2+} sparks evoked by action potentials in mouse ventricular myocytes. The Journal of Physiology. 1999; 518:469-478

Buckwalow IB, Böcker W. (2010) Immunohistochemistry: Basics and Methods. Springer-Verlag Berlin Heidelberg

Carey GB. The swine as a model for studying exercise-induced changes in lipid metabolism. Medicine & Science in Sports & Exercise. 1997; 29(11):1437-43

Contreras-Ferrat AE, Toro B, Bravo R, Parra V, Vásquez C, Ibarra C, Mears D, Chiong M, Jaimovich E, Klip A, Lavandero S. An inositol 1,4,5-triphosphate (IP_3)-IP_3 receptor pathway is required for insulin-stimulated glucose transporter 4 translocation and glucose uptake in cardiomyocytes. Endocrinology. 2010; 151(10)4665-77

Cordiero JM, Spitzer KW, Giles WR, Ershler PE, Cannell MB, Bridge JHB. Location of the initiation site of calcium transients and sparks in rabbit heart Purkinje cells. Journal of Physiology. 2001, 531.2; 301-314

Crick SJ, Sheppard MN, Ho SY, Anderson RH. Localization and quantitation of autonomic innervation in the porcine heart I: conduction system. Journal of Anatomy. 1999;195:341-57

Davidenko J, Delmar M, Oates R, Jalife J. Electrophysiological actions of dantrolene sodium in isolated sinoatrial and atrioventricular nodes and in a model of ischemia. Journal of Pharmacology and Experimental Therapeutics. 1986; 238(1):206-16

Dawson B and Trapp RG. (2001) Basic & Clinical Biostatistics. 3rd Edition. United States of America. The McGraw-Hill Companies, Inc.

Di Maio A, ter Keurs HE, Franzini-Armstrong C. T-tubule profiles in Purkinje fibres of mammalian myocardium. Journal of Muscle Research and Cell Motility. 2007; 28(2-3):115-21(a)

Di Maio A, Karko K, Snopko RM, Meija-Alvarez R, Franzini-Armstrong C. T-tubule formation in cardiac myocytes: two possible mechanisms? Journal of Muscle Research and Cell Motility. 2007; 28(4-5):231-41(b)

FEI Company. All that you wanted to know about electron microscopy: but didn't dare to ask. 2006 [Accessed July 4, 2010. Available at: http://www.fei.com/uploadedFiles/Documents/Content/2006_06_AllYouWanted_pb.pdf]

Forthofer RN, Lee ES, Hernandez M. (2007). Biostatistics. A guide of design, analysis and discovery. 2nd Ed. Oxford, UK. Elsevier Inc.

Grant DM, McGinty J, McGhee EJ, Bunney TD, Owen DM, Talbot CB, Zhang W, Kumar S, Munro I, Lanigan PM, Kennedy GT, Dunsby C, Macgee AI, Courtney P, Katan M, Neil MA, French PM. High speed optically sectioned fluorescence lifetime imaging permits study of live cell signaling events. Optics Express. 2007; 15(24):15656-73

Guthoff RF, Zhivov A, Stachs O. In vivo confocal microscopy, an inner vision of the cornea- a major review. Clinical and Experimental Ophthamology. 2009; 37(1):100-17

Heart & Stroke Foundation of Canada. Statistics (2008) Available at: http://www.heartandstroke.com/site/c.ikIQLcMWJtE/b.3483991/k.34A8/Statistics.htm#heartdisease [Accessed 11, April 2012]

Hirose M, Stuyvers BD, Dun Wen, ter Keurs HEDJ, Boyden P. Function of Ca^{2+} release channels in Purkinje cells that survive in the infarcted canine heart: a mechanism for triggered Purkinje ectopy. Circulation: Arrhythmia Electrophysiology. 2008; 1:387-395

Hirose M, Stuyvers B, Dun W, ter Keurs H, Boyden PA. Wide long lasting perinuclear $Ca2^{+}$ release events generated by an interaction between ryanodine and IP_3 receptors in canine Purkinje cells. Journal of Molecular and Cellular Cardiology. 2008; 45(2):176-84

Huiikuri HV, Castellanos A, Myerburg RJ. Sudden Death due to Cardiac Arrhythmias. New England Journal of Medicine. 2001; 345(20):1473-82

Jaffe, LF. On the conservation of fast calcium wave speeds. Cell Calcium. 2002; 32(4): 217–229

Jiang D, Xiao B, Chen SR. Smooth muscle tissues express a major dominant negative splice variant of the type 3 Ca^{2+} release channel (ryanodine receptor). The Journal of Biological Chemistry. 2003; 278(7): 4763-9

Katz AM.(1992) Physiology of the Heart. New York, New York. Raven Press Books Ltd.

Kong H, Jones PP, Koop A, Zhang L, Duff HJ, Chen SRW. Caffeine Induces Ca2+ Release by Reducing the Threshold for Luminal Ca^{2+} Activation of the Ryanodine Receptor. Biochemical Journal 2008; 414(3):441-452

Krause T, Gerbershagen MU, Feige M, Weißhorn R and Wappler F. Dantrolene-A review of its pharmacology, therapeutic use and new developments. Anesthesia. 2004; 59: 364-373

Kumar S, Kasseckert S, Kostin S, Abdallah Y, Schafer C, Kaminski A, Reusch HP, Piper HM, Steinhoff G, Ladilov Y. Ischemic acidosis causes apoptosis in coronary endothelial cells through activation of caspase-12. Cardiovascular Research 2007; 73(1):172-80

Legato MJ. Ultrastructure of the atrial, ventricular, and Purkinje cell, with special reference to the genesis of arrhythmias. Circulation. 1973; 47(1): 178-89

Luo DL, Gao J, Lan XM, Wang G, Wie S, Xiao RP, Han QD. Role of inositol 1,4,5-trisphosphate receptors in alpha1-adrenergic receptor-induced cardiomyocyte hypertrophy. Acta Pharmacologica Sinica. 2006; 27(7):895-900.

Narasimhan K, Pessah IN, Linden DJ. Inositol-1,4,5-triphosphate receptor-mediated Ca mobilization is not required for cerebellar long-term depression in reduced preparations. Journal of Neurophysiology. 1998; 80(6):2963-74.

NIST/SEMATECH e-Handbook of Statistical Methods. NIST is an agency of the US Commerce Department's Technology Administration. Last updated April 2012. Accessed: June 20, 2012. Available at: http://www.itl.nist.gov/div898/handbook/index.htm

Murayama T, Oba T, Katayamas E, Oyamada H, Oguchi K, Kobayashi M, Otsuka K, Ogawa Y. Further characterization of the Type 3 Ryanodine Receptor (RyR3) Purified from Rabbit Diaphragm. The Journal of Biological Chemistry 1999 ; 274(24):17297-17308

Peters SC, Piper HM. Reoxygenation-induced Ca^{2+} rise is mediated via Ca^{2+} influx and Ca2+ release from the endoplasmic reticulum in cardiac endothelial cells. Cardiovascular Research. 2007; 73(1) 164-71

Reddy KS, Yasuf, S. Emerging epidemic of cardiovascular disease in developed countries. Circulation. 1998; 97:596-601

Saggau P. New methods and uses for fast optical scanning. Current Opinion in Neurobiology. 2006;16:543-550.

Salata JJ, Jalife J. Effects of dantrolene sodium on the electrophysiological properties of canine cardiac Purkinje fibers. The Journal of Pharmacology and Experimental Therapeutics. 1982; 220(1):157-66

Salata JJ, Jalife J. Dantrolene Sodium: Effects on Isolated Cardiac Tissues. Journal of Molecular and Cellular Cardiology. 1983; 15:233-243

Sobie EA, Guatimosim S, Gomez-Viquez L, Song LS, Hartmann H, Saleet Jafri M, Lederer WJ. The Ca2+ leak paradox and rogue ryanodine receptors: SR Ca^{2+} efflux theory and practice. Progress in Biophysical and Molecular Biology. 2006; 90(1-3):172-185

Sommer and Johnson. Cardiac Muscle. A Comparative Study of Purkinje Fibers and Ventricular Fibers. The Journal of Cell Biology. 1968; 36(3):497-526

Spitzer KW, Cordiero JM, Ershler PR, Giles W, Bridge JHB. Confocal microscopy reveals that calcium transients in Purkinje myocytes are initiated at the cell periphery. Circulation. 1997; 96 (suppl 1) 1-239. Abstract

Stuyvers BD, Boyden PA, ter Keurs HE. Calcium Waves: physiological relevance in cardiac function. Circulation Research. 2000; 86(10):1016-8

Stuyvers BD, Dun W, Matkovich S, Sorrentino V, Boyden PA, ter Keurs HE. Ca^{2+} sparks and waves in canine Purkinje cells: a triple layered system of Ca^{2+} activation. Circulation Research. 2005;97(1):35-43

Szumowski L, Sanders P, Walczak F, Hocini M, Jaïs P, Kepski R, Szufladowicz E, Urbanek P, Derejko P, Bodalski R, Haïssaguerre M. Mapping and ablation of Polymorphic Ventricular Tachycardia after Myocardial Infarction. Journal of the American College of Cardiology. 2004; 44(8): 1700-6

Williams DB and Carter CB. (1996) Transmission Electron Microscopy: A Textbook for Materials Science. New York, New York. Plenum Press.

Wilkins, A. Techniques in Neuroscience: Immunohistochemistry. Advances in Clinical Neuroscience and Rehabilitation (ACNR). 2005; 5(5):29-30

Zipes DP, Wellens HJ. Sudden Cardiac Death. Circulation..1998; 98(21):2234-51

Zhou F, Li P, Chen SR, Louis CF, Fruen BR. Dantrolene inhibition of ryanodine receptor Ca^{2+} release channels. Molecular mechanism and isoform selectivity. The Journal of Biological Chemistry. 2001; 276(17): 13810-6

Yokogawa Electric Corporation. CSU10. 1994-2012. Accessed June 20, 2012. Available at: http://www.yokogawa.com/scanner/products/csu10e.htm

Zucchi R, Ronca-Testoni S. The sarcoplasmic reticulum Ca2+ channel/ryanodine receptor: modulation by endogenous effectors, drugs and disease states. Pharmacological Reviews. 1997; 49(1): 1-51